UCRL-ID-119912

# Documentation Concerning KKP Development Work

S. Dixit

December 22, 1994

Lawrence Livermore National Laboratory

Work performed under the auspices of the U.S. Department of Energy by the Lawrence Livermore National Laboratory under Contract W-7405-ENG-48.

This report has been reproduced
directly from the best available copy.

Available to DOE and DOE contractors from the
Office of Scientific and Technical Information
P.O. Box 62, Oak Ridge, TN 37831
Prices available from (615) 576-8401, FTS 626-8401

Available to the public from the
National Technical Information Service
U.S. Department of Commerce
5285 Port Royal Rd.,
Springfield, VA 22161

# Documentation Concerning KKP Development Work

S. Dixit

***Laser Science and Technology Program***

*Mail Station L-493*

*Ext: 3-7321*

February 20, 1994

To: Distribution

S.D.

From: Sham Dixit, Ian Thomas, Mike Rushford and Ray Merrill RM

Subject: 16 level kinoform phase plate (KPP) fabricated in fused silica using lithographic methods and wet etching

## Summary

We have fabricated a 16 level KPP on a 5" diameter aperture fused silica using lithographic techniques and wet etching of fused silica in a buffered hydrofluoric acid solution. The experimentally measured far-field intensity pattern displays the desired top-hat envelope and has a superimposed speckle on it. The far-field contains 90% of the incident energy inside the 640 μm region. This is a significant improvement over the binary RPP's in terms of the far-field profile control and energy concentration. Sources contributing to the energy loss are identified and efforts are underway to overcome these limitations.

## Introduction

In an earlier memo [1] it has been shown that continuous contour phase plates (which we call kinoform phase plates or KPPs) offer significant advantages over the commonly used binary random phase plates (RPP's). The KPPs allow complete flexibility in tailoring the far-field profile with most of the incident energy contained inside the desired region. Our simulations have shown that one can easily produce top-hat supergaussian intensity profiles in the far-field that contain more that 95% of the incident energy inside the central spot.

For the last year and a half we (the authors of this memo and Janice Lawson and Amber Morgan who worked on the early investigations of KPP fabrication) have been examining different methods for fabricating the KPP's for high power applications such as on Nova and on the proposed NIF. We have now fabricated a 16 level KPP on a 5" diameter aperture fused silica using lithographic techniques and wet etching of fused silica in a buffered hydrofluoric acid solution. The KPP phase profile is etched directly into fused silica and hence the finished product is expected to have high laser damage threshold at 3ω. The experimentally measured far-field intensity pattern displays the desired top-hat envelope and has superimposed speckle on it.

***University of California***

**Lawrence Livermore**
**National Laboratory**

The far-field contains 90% of the incident energy inside the 640 μm region. This is a significant improvement over the binary RPP's in terms of the far-field profile control and energy concentration. Sources contributing to the energy loss are identified and efforts are underway to overcome these limitations.

## Design of the test KPP

We used the iterative algorithm described in [1] to construct the kinoform phase screen. The KPP was designed to produce a 640 μm diameter 8-th power super-Gaussian intensity profile when used at 2ω with a 3m focal length lens. The calculated phase screen is shown in figure 1 after it has been discretized to 16 levels. We did a sensitivity study to the level of discretization and estimate that 16 level discretization leads to ~ 1% energy loss outside the desired region compared to the continuous phase limit. The pixel size was 305 μm and the KPP spanned 410 pixels in diameter so that the KPP size was about 12.5 cm or 5" in diameter. Since the first zero in the $\mathrm{Sinc}^2$ pattern for a 305 μm square aperture occurs at ~ 5mm from the center, we believe that the aliasing errors would be greatly reduced and the energy distribution should resemble that for a continuous phase screen.

## KPP Fabrication

The KPP was fabricated using lithographic techniques. Here $2^N$ phase levels can be fabricated using N binary amplitude masks and varying etch times for each mask. Thus four masks are needed for producing a 16 level KPP. The masks for various exposure stages are generated by sorting out the binary indices for the phase levels in a binary representation. For example, a phase level 13 (= 1101 base 2) implies a 1 for mask 1, 1 for mask 2, a 0 for mask 3 and a 1 for mask 4. Note that a 1 in the mask implies an etch and a zero implies no etch.

A 2π phase optical phase delay corresponds to an etch depth of $t = \lambda/(n-1)$ where n is the refractive index at the operating wavelength λ. In the multiple binary mask approach, etching following exposure through mask 1 is for a depth t/2, that following mask 2 is for a depth t/4, the next one for t/8 and so on. At the end of the procedure one ends up with $2^N$ phase levels ( 0 to $2^N-1$) with a maximum etch depth of $t\,(2^N-1)/2^N$ . For the 2ω test KPP, t = 1171 nm so that the smallest etching step is for a depth of 73.2 nm. Thus level 13, for example, achieves its depth via the etches for masks 1,2 and 4 [ depth= $t(1/2+1/4+1/16) = t\,13/16$]. The binary amplitude masks for each exposure stage were prepared using a Gerber plotter on acetate film.

With the four binary masks prepared as described above, the fabrication of the 16 level KPP proceeded as follows. Approximately 120 nm of chrome was deposited on 0.5 inch thick, 6 inch diameter fused silica substrates prior to the KPP fabrication. We found that the surface must be very clean to ensure a good adhesive bond with the photoresist and thus avoid undercutting and peeling during the subsequent etching. This cleaning was carried out by exposing the substrate to hard UV light in the presence of air (liberating ozone). We also found that use of an adhesion promoter, hexamethyldisilizane (HMDS), increased the strength of the photoresist-substrate bond.

The kinoform fabrication was carried out is steps as follows:

1. UV/O3 cleaning of the substrate
2. Spin on adhesion promoter and air dry for 60 secs.
3. Spin on Shipley 1400 photoresist
4. Soft bake at 80° C for 30 mins.
5. Expose through the first mask
6. Develop the pattern
7. Hard bake at 120° C for 60 mins.
8. Etch off the exposed chrome
9. Etch exposed silica in 1% HF/15% $NH_4F$ aqueous solution at 24° C for 28 mins.
10. Remove photoresist by washing in base.

The above steps were repeated for each of the remaining masks with the etch times in step 9 being reduced by a half in each subsequent step (14 min, 7 min and 3.5 min for masks 2,3 and 4 respectively). These etch times were calculated from a predetermined etch rate of 20.6 nm/min and corresponded to successive etch depths of 578nm, 289 nm, 145nm and 72.5 nm.

Accurate overlay of masks is crucial to obtaining sharp edges between the pixels on the KPP. Wider edges lead to large angle scattering and hence to a reduction in the amount of energy contained inside the central top-hat profile. We aligned the masks using three alignment fiducials placed at the edge of the KPP pattern. The fiducials on masks 2, 3 and 4 were aligned, prior to exposure, with those initially patterned on the substrate from mask 1.

At the end of the four etch steps, the small amount of chrome remaining on the surface was removed and the sample was then ready for evaluation.

## Characterization of the KPP

At the end of the fabrication, there would be 16 phase steps in the fused silica substrate. During the preparation of the masks, we had placed calibration strips at four places on the film. A white light interferogram of a section of a KPP, shown in figure 2, clearly displays the various phase levels on the calibration strip as well as on the KPP through different colors. We measured the etch depths of different phase levels using a Dektak stylus profilometer. The average step heights measured over the four calibration strips are compared with the desired step heights in figure 3. The maximum deviation is about 9% although most of the steps are within ± 4% of the desired thickness.

Accurate overlay of the multiple masks is of critical importance to obtaining a high performance of a KPP. We found that the masks made on acetate film lead to considerable uncertainty in preserving the alignment accuracy across the KPP aperture. High resolution microscope pictures of the edges indicated that some of the edges were very sharp (better than 2 μm) while others were very broad (as much as 20 μm with staircase like features where multiple masks were exposed). We are currently working on the precision alignment of the multiple masks. The misalignment of masks leads to a reduction in the KPP efficiency without significantly altering the far-field intensity profile. Based on simple area arguments, if all the edges were 5 μm wide, this would lead to a 3% loss in the energy efficiency due to wide angle scattering.

## Optical performance of the KPP

We evaluated the performance of the KPP by measuring the far-field intensity profile and the energy contained in it. The monochromatic output of an argon-ion laser at 514 nm was collimated, passed through the KPP and focused using a 3m focal length lens. The difference between 514 and 527 nm is not expected to make a significant difference in the measurements. The far-field image was recorded on film, digitized using a photodensitometer and the digitized image was processed on the computer to calculate the intensity. One such processed focal plane intensity profile is shown in figure 4. The intensity pattern has the required top-hat envelope of ~ 640 μm diameter with a superimposed speckle pattern. We believe the speckle pattern is a consequence of aberrations in the beam due to air turbulence etc. The speckle pattern can be smoothed using any one of the temporal smoothing techniques.

In addition to the desired top-hat profile at the center, we also observed a halo around this and also the diffraction pattern of the individual 305 μm pixels extending to several orders in the horizontal and the vertical directions. These features are at much lower intensities compared to the desired central spot. The features due to diffraction around a pixel can be eliminated by fabricating a continuously varying phase screen (as opposed to the pixelated one fabricated here). We believe the halo can be eliminated by sharpening the KPP pixel edges. Fabrication of the same KPP pattern with <1μm edge width is currently underway.

The energy concentration in the focal plane was calculated by measuring the energy passing through pinholes of differing sizes normalized to the energy transmission in the absence of the KPP. This is compared with the theoretical energy distribution in figure 5. We see that the measured fractional energy values follow closely the theoretical values but seem to be about 5% below them. We believe some of this deviation is due to poor edge definition. Nevertheless, we see that the 640 μm diameter region contains approximately 90% of the incident energy. This is a significant improvement over the binary RPP energy content of 82%.

In summary, we have fabricated a 16 level KPP on a 5" diameter aperture fused silica using lithographic techniques and wet etching of fused silica in a buffered hydrofluoric acid solution. The experimentally measured far-field intensity pattern displays the desired top-hat envelope and has a superimposed speckle on it. The far-field contains 90% of the incident energy inside the 640 μm region. This is a significant improvement over the binary RPP's in terms of the far-field profile control and energy concentration.

We are currently working on improving the efficiency of the KPP. At the same time, we are also developing methods for scale-up of the technology for fabricating KPP's for use on Nova (65cm diameter) and on the proposed NIF (40 cm square).

## Reference

[1] "Continuous contour (kinoform) phase plates", internal memorandum by Sham Dixit November 20, 1992

## Figure captions

Figure 1 Calculated KPP phase screen for producing a 640 μm top-hat intensity profile in the far-field. KPP is to used at 2ω with a 3m focal length lens.

Figure 2. A white light interferogram of the KPP. Note the various phase levels (as indicated by the different colors) on the calibration strip and also on the KPP (area below the circular arc).

Figure 3. Comparison of the measured phase step heights (dashed lines) with the required ones (solid lines). The ratio of the experimental to the desired step heights is shown against each level.

Figure 4. Measured far-field intensity distribution produced by the KPP.

Figure 5. Energy concentration in the far-field produced by the KPP. The data points denoted by an asterisk correspond to the fractional energy passing through a pinhole placed at the primary focus; those marked by a diamond taken with the same set of pinholes at a 2X magnified image of the far-field spot; the crosses are with 4X magnification. The solid line denotes the theoretical energy concentration.

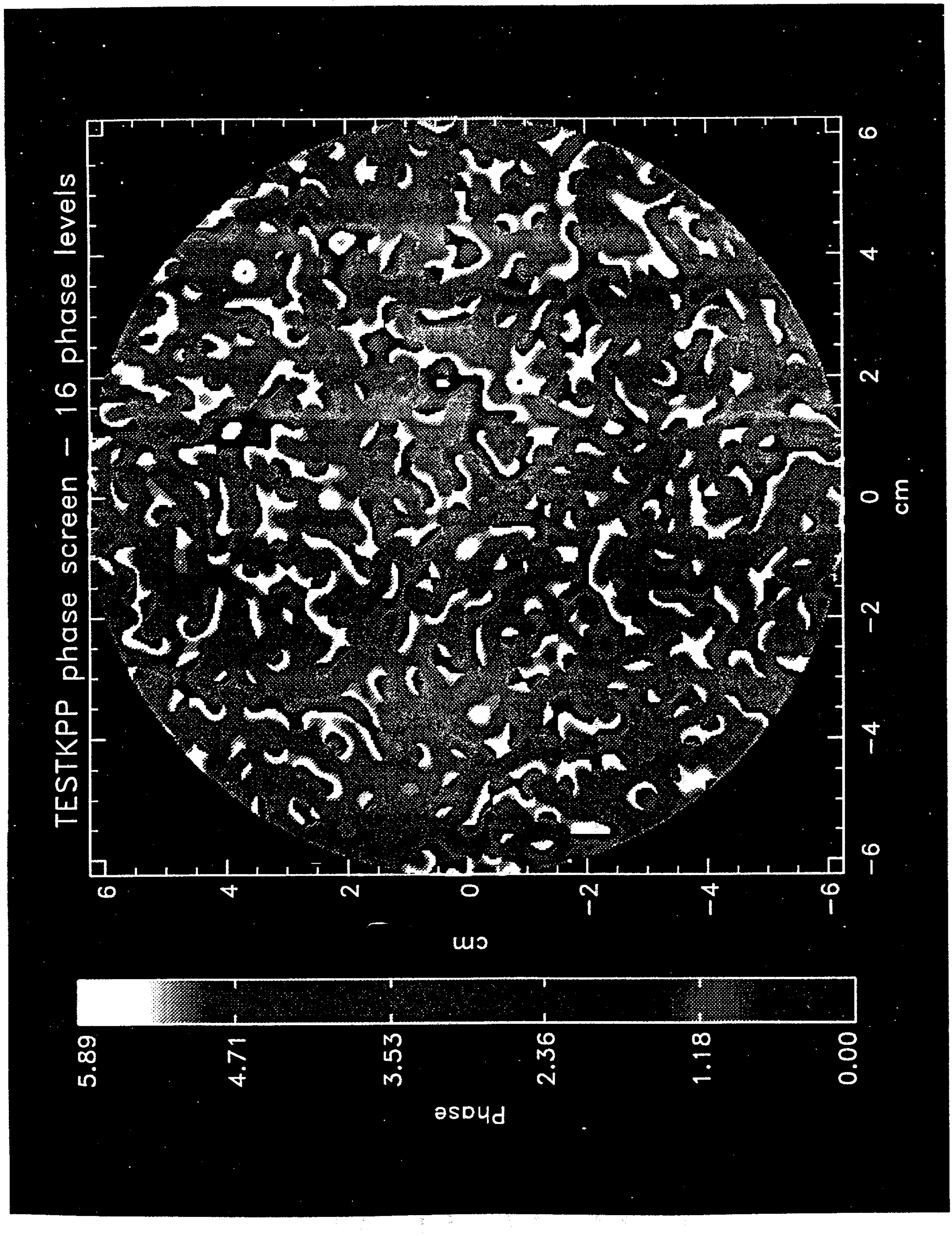

TESTKPP phase screen — 16 phase levels
cm
-6
-4
-2
0
2
4
6
cm
6
4
2
0
-2
-4
-6
Phase
5.89
4.71
3.53
2.36
1.18
0.00

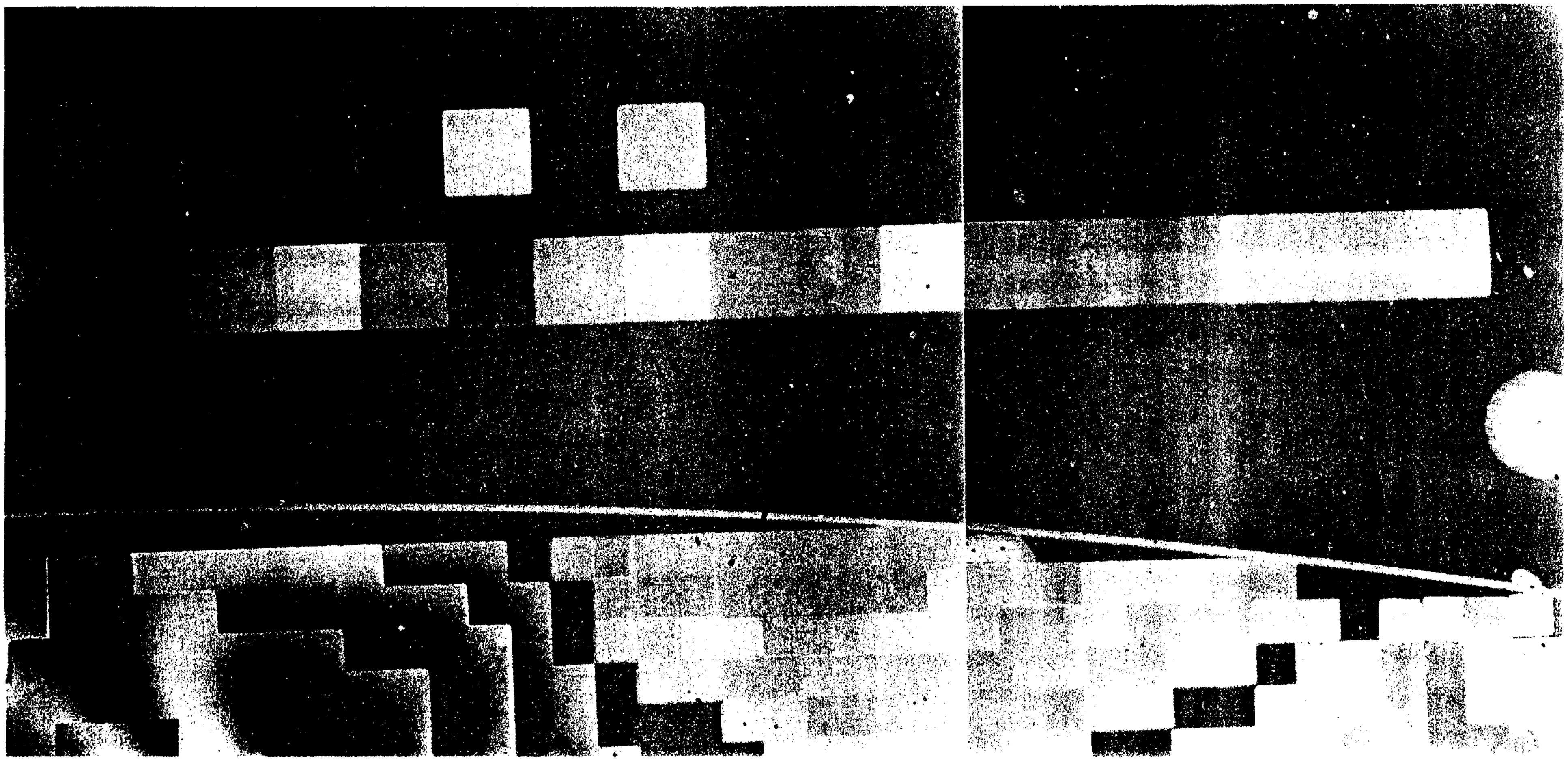

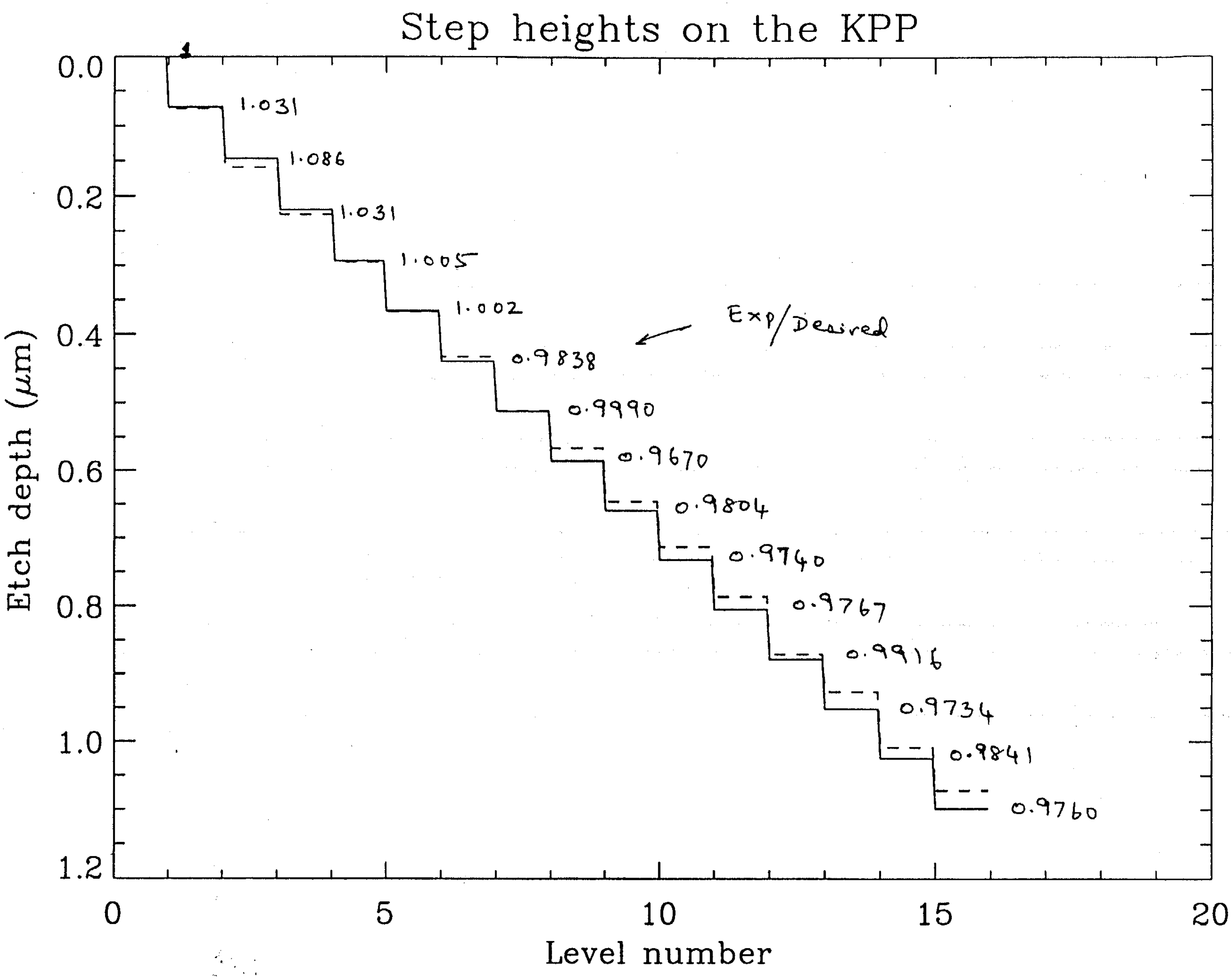
Step heights on the KPP
Etch depth (μm)
0.0
0.2
0.4
0.6
0.8
1.0
1.2
Level number
0
5
10
15
20
1.031
1.086
1.031
1.005
1.002
0.9838
0.9990
0.9670
0.9804
0.9740
0.9767
0.9916
0.9734
0.9841
0.9760
Exp/Desired

Figure 7

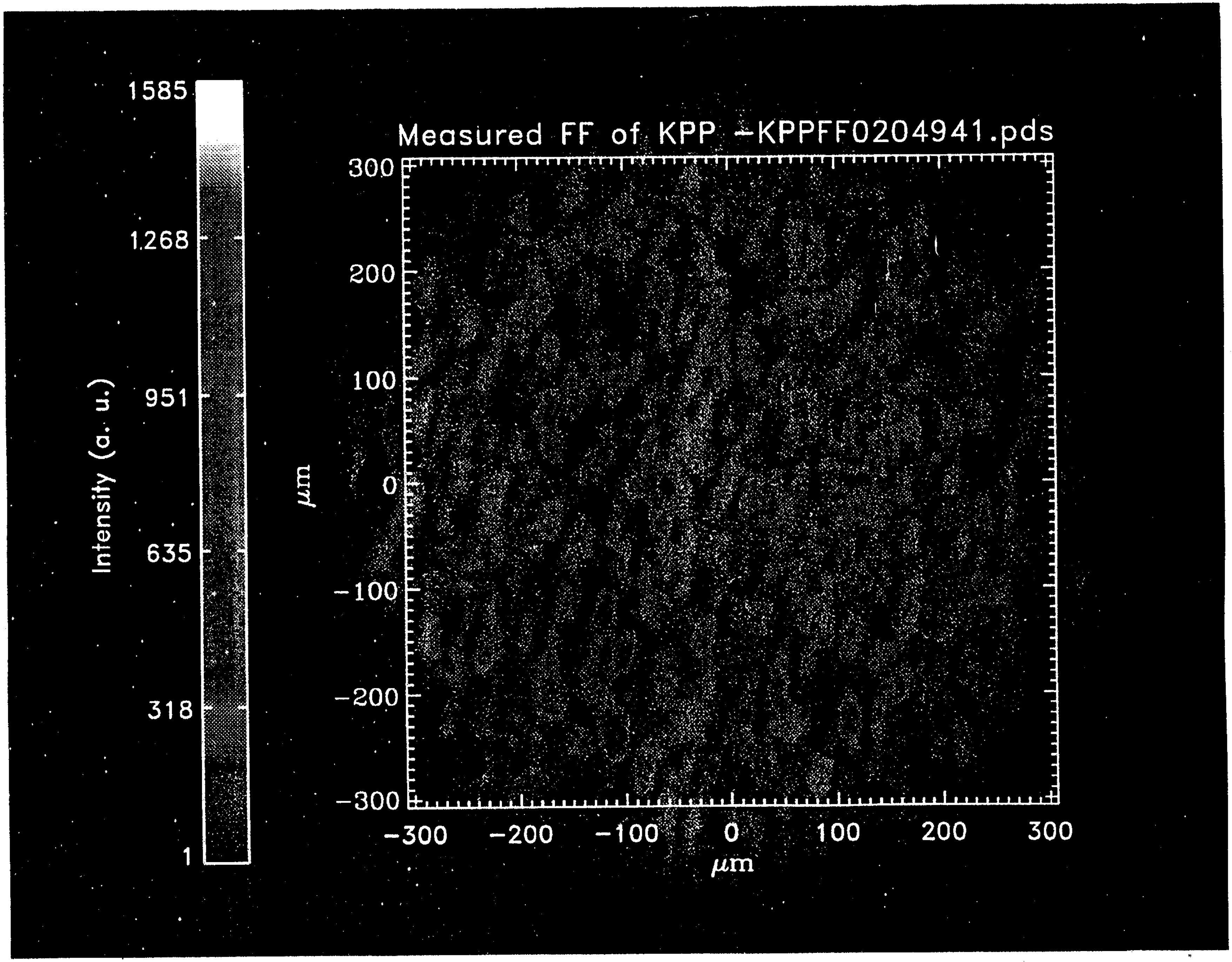
Measured FF of KPP -KPPFF0204941.pds
Intensity (a. u.)
1585
1,268
951
635
318
1
μm
300
200
100
0
−100
−200
−300
−300
−200
−100
0
100
200
300
μm

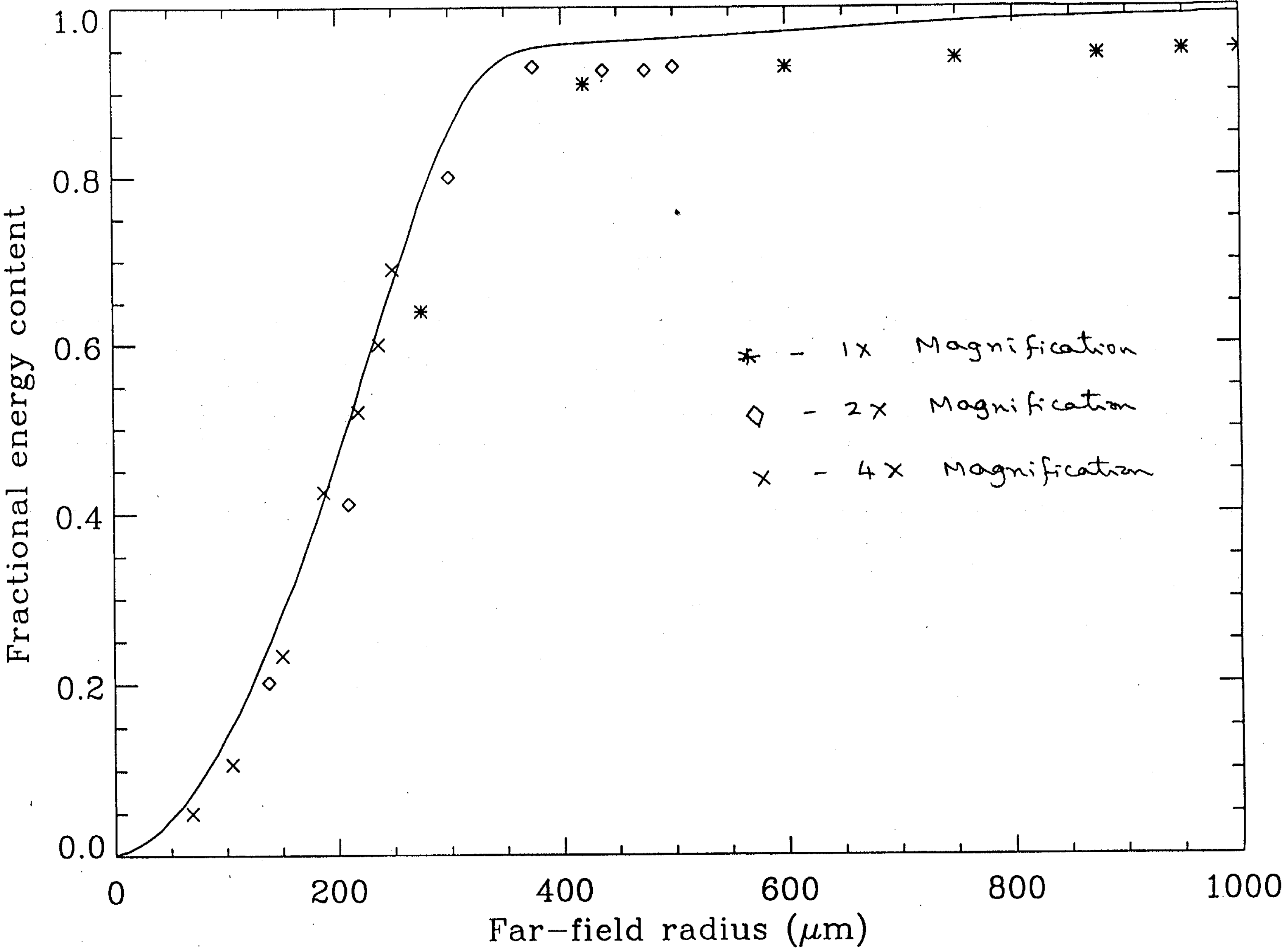

KPP far-field energy concentration

***Laser Science and Technology Program***

*Mail Station L-493*

*Ext: 3-7321*

February 22, 1994

To: Distribution

From: Sham Dixit and Mike Feit

Subject: Near-field diffraction from KPP edges

Kinoform phase plates (KPPs) based on computer generated designs consist of pixelated phase values over the substrate. For convenience of fabrication using lithographic methods, the phase values are also discretized into a finite number of levels. When the KPPs are used in the laser beam, diffraction around these discrete, pixelated phase regions is expected to lead to intensity modulations which could induce damage in the debris shield if the KPP is fabricated on the input side of the debris shield. While placing the KPP on the target side of the debris shield would alleviate any potential damage induced by diffraction, this latter arrangement may lead to complications with regard to debris shield maintenance on NIF.

In order to assess the extent of the intensity enhancement, we have performed near-field diffraction calculations around a KPP phase edge. Note that we are primarily interested in intensity modulations from the KPP surface to about 1 cm from it (thickness of the debris shield). For these distances, there is minimal 'cross talk' between the diffraction from neighboring pixels (pixel size ~ 1mm) and we need be only concerned about the diffraction from around a single phase jump such as that shown in figure 1. The edge, represented as two semi-infinite constant phase regions connected by a ramp, is characterized by the transition width (a) and the phase step height ($\phi$).

Diffraction around a linear one-dimensional ramp can be calculated analytically in terms of the Fresnel cosine and sine integrals. Following the methods discussed in Born and Wolf, the result for the transmitted electric field amplitude is

***University of California***

**Lawrence Livermore**
**National Laboratory**

$$U(p) = \frac{1}{1+i}\Big[\Big\{\frac{1}{2} - C(p+\frac{a_0}{2})\Big\} + i\Big\{\frac{1}{2} - S(p+\frac{a_0}{2})\Big\} + e^{i\phi}\Big\{\frac{1}{2} + C(p-\frac{a_0}{2})\Big\} + i\Big\{\frac{1}{2} + S(p-\frac{a_0}{2})\Big\} + e^{i\frac{\phi}{2}+i\frac{\pi}{2}(2p\beta-\beta^2)}\Big\{ C(p-\beta+\frac{a_0}{2}) - C(p-\beta-\frac{a_0}{2}) + i\Big\{ S(p-\beta+\frac{a_0}{2}) - S(p-\beta-\frac{a_0}{2})\Big\}\Big\}\Big] \qquad (1)$$

where the normalized variables p, $a_0$ and $\beta$ are defined as

$$p = x\sqrt{\frac{2}{\lambda z}}\,,\ a_0 = a\sqrt{\frac{2}{\lambda z}} \text{ and } \beta = \frac{\phi}{a_0}\frac{2}{\pi}. \qquad (2)$$

The Fresnel C and S integrals are defined as

$$C(x) + i\,S(x) = \int_0^x e^{i\frac{\pi}{2}\xi^2}\,d\xi. \qquad (3)$$

The diffracted intensity is given by

$$I(p) = |U(p)|^2. \qquad (4)$$

In Eq. (1) the first two terms describe the diffraction around a phase jump while the third term describes the effect of the ramp. Note that as z becomes large, $\beta$ increases while $a_0$ decreases. For distances $z >> a^2/\lambda$ the last term becomes small and the diffraction pattern resembles that of the sharp edge.

In figure 2, we show the intensity enhancement due to Fresnel diffraction from a sharp phase step (a = 0). In the paraxial limit, the enhancement is independent of the propagation distance. We see that the enhancement is peaked at 1.8 when the phase step height is $\pi$ and is symmetric in $\phi$ around it. This result can also be shown analytically from Eq. (1). Such near-field enhancements have been observed for binary RPP's on Nova. These results also imply that a sufficient number of levels (32 or higher) is necessary in order to maintain small phase step heights and in turn keep the intensity modulation low (below ± 10%).

While the above calculations are for infinitesimally thin edges, practical limitations on fabrication always produce edges of finite width. For example, the sol-gel binary phase plate elements have been measured to have edges that are about 5-7 μm wide. Thus the question arises as to the effect of diffraction around the finite width of the transition region ($a \neq 0$) on the intensity enhancement. Figures 3-5 show contour maps of peak intensity as a function of the phase step height and the transition width at 3 mm, 7 mm and 1 cm from the edge (free space propagation distance). We assume $\lambda = 351$ nm in all these calculations. Although these figures look complicated, several systematics are evident:

- Intensity enhancement is small and nearly insensitive to a for small phase steps.
- $\pi$ phase steps show large and mildly sensitive intensity enhancements.
- For phase steps around $2\pi$, the peak intensity increases for wider edges and for shorter distances of propagation.

These results suggest that if we wish to limit the intensity enhancements to 10-15%, the edge width has to be about 1 μm or smaller and there has to be a sufficient number of phase levels in the kinoform. Edge definitions of 1 μm a have recently been demonstrated by Ian Thomas by HF etching of fused silica and submicron edge definitions are routinely achieved in the semiconductor industry by e-beam and UV lithography and reactive ion etching. A 1 μm edge resolution is also commonly achieved in integrated micro-optics/diffractive optical element fabrication. Thus we are confident that the tolerance implied by these results is achievable with currently available technology. Recent calculations by Ken Manes for a 10 μm wide $2\pi$ jump show ~1.7:1 enhancement within a few millimeters of propagation, in reasonable agreement with the results in figs 3-5. However, it is clear from our calculations that making finer edges (~ 1 μm wide) minimize the enhancement in this region.

The fact that the peak intensity increases for $2\pi$ jumps closer to the edge raises an intriguing (and possibly worrisome) question: does the enhancement keep on increasing as we get closer to the edge? If so, is there a maximum peak enhancement? Since the paraxial approximation breaks down near the edge, one has to solve the full Helmholtz equation to calculate diffraction. In this case the diffracted field is given by the integral

$$U(x,y) = \int A(u,v)\, du\, dv\, e^{\left\{i\, 2\pi\, (xu+yv)\right\}}\, e^{\left\{i\, 2\pi \frac{z}{\lambda}\left[1 - (\lambda u)^2 - (\lambda v)^2\right]^{1/2}\right\}} \qquad (5)$$

where the angular plane wave spectrum A(u,v) can be related to the incident field (including the phase jump) E(x,y) through

$$E(x,y) = \int A(u,v)\, du\, dv\, e^{\{i\, 2\pi\, (xu+yv)\}} . \qquad (6)$$

We have calculated the diffracted intensity for a 1 μm wide edge using FFT techniques. The results for the peak intensity are displayed in figure 6 for phase steps of 0.05π, π and 2π. We see that while small phase jumps are benign, ≈ 2π jumps lead to ~ 3.5:1 modulations within a few μm following the edge. We have verified that the enhancement quickly subsides to 10% within 1 mm following the edge.

Thus it seems that highest enhancement occurs within ~ 10 μm or so from the phase step, a distance of the order of a Fresnel length for a 1 μm edge. We are presently measuring the optical damage due to diffraction around individual phase jumps. It is also worth noting that such near-field enhancements, which also ought to be occurring in the sol-gel phase plates used extensively on Nova, have so far not caused any damage to the debris shields that is reminiscent of the phase plate element boundaries.

There are several ways of circumventing/overcoming this potential threat on NIF. Some of these are:

i) place the KPP on the target side of the debris shield. This is by far the easiest solution provided other constraints with regard to the debris shield handling/cleaning could be accommodated.

ii) place the KPP on the output surface of the final focus lens (this solution was sugested by Mike Perry). While this protects against the enhancements occurring immediately following the phase step, a potential optical damage could occur at the debris shield because of the residual modulations persisting several centimeters past the phase step. Figure 7 shows the amount of such modulation for distances of upto 5 cm following a 1 μm wide phase step. Note that for 1 mm size pixels, there is still negligible cross-talk between different phase steps (Fresnel distance corresponding to 1 mm is 300 cm). Hence single edge diffraction dominates for these distances. We see that with enough phase levels, the modulation from straight edges could be contained to 10-15%. Diffraction around the corners would give

We see that with enough phase levels, the modulation from straight edges could be contained to 10-15%. Diffraction around the corners would give somewhat higher modulations. (These calculations are in progress.) This option would require development of technologies for fabricating the KPP's on the curved lens surface.

iii) construct KPP designs which have a truly continuous phase without any phase jumps. We are investigating such designs. Fabrication of such KPP's requires forming continuous phase contours in thick photoresist coatings and (almost certainly) reactive ion etching these into fused silica.

Figure capions:

Figure 1. Variation of the phase across a phaseplate element boundary. a denotes the width of the transition region and $\phi$ the height of the phase step.

Figure 2. Intensity enhancement (normalized to the incident intensity) in the diffraction following a sharp phase step. The maximum (solid line) and the minimum (dashed line) in the diffracted intensity pattern are plotted for different values of the phase step. Note that for sharp edges, the values of the intensity maximum and minimum are independent of the propagation distance.

Figure 3. Intensity enhancement for finite width phase step. The contour lines represent the peak values in the diffracted intensity pattern at $z = 3$ mm. They are plotted for different transition widths and phase step heights.

Figure 4. Same as figure 3 except for $z = 7$ mm.

Figure 5. Same as figure 3 except for $z = 10$ mm.

Figure 6. Peak intensity at close proximity to a 1 μm wide phase step. These calculations are done in the non-paraxial limit by solving the Helmholtz equation.

Figure 7. Dependence of the peak intensity on the propagation distance. The phase transition region is assumed to be 1 μm wide. These calculations are done within the paraxial limit. Note that after the transients due to the transition region have dissipated away, the peak intensity becomes independent of z and reaches the values for a sharp phase step given in figure 1.

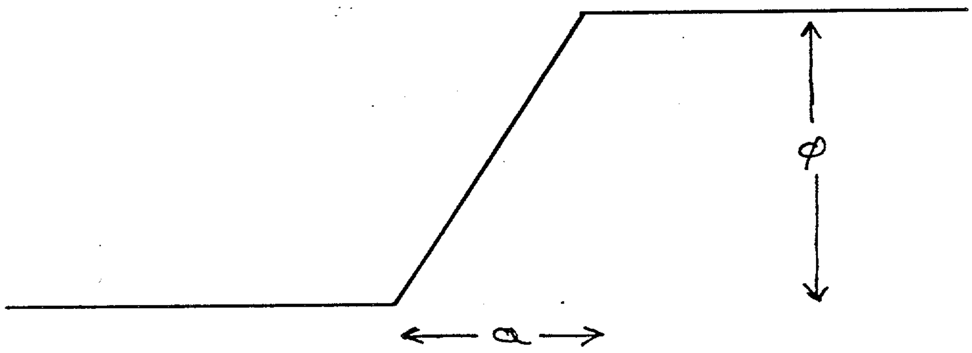

Figure 1

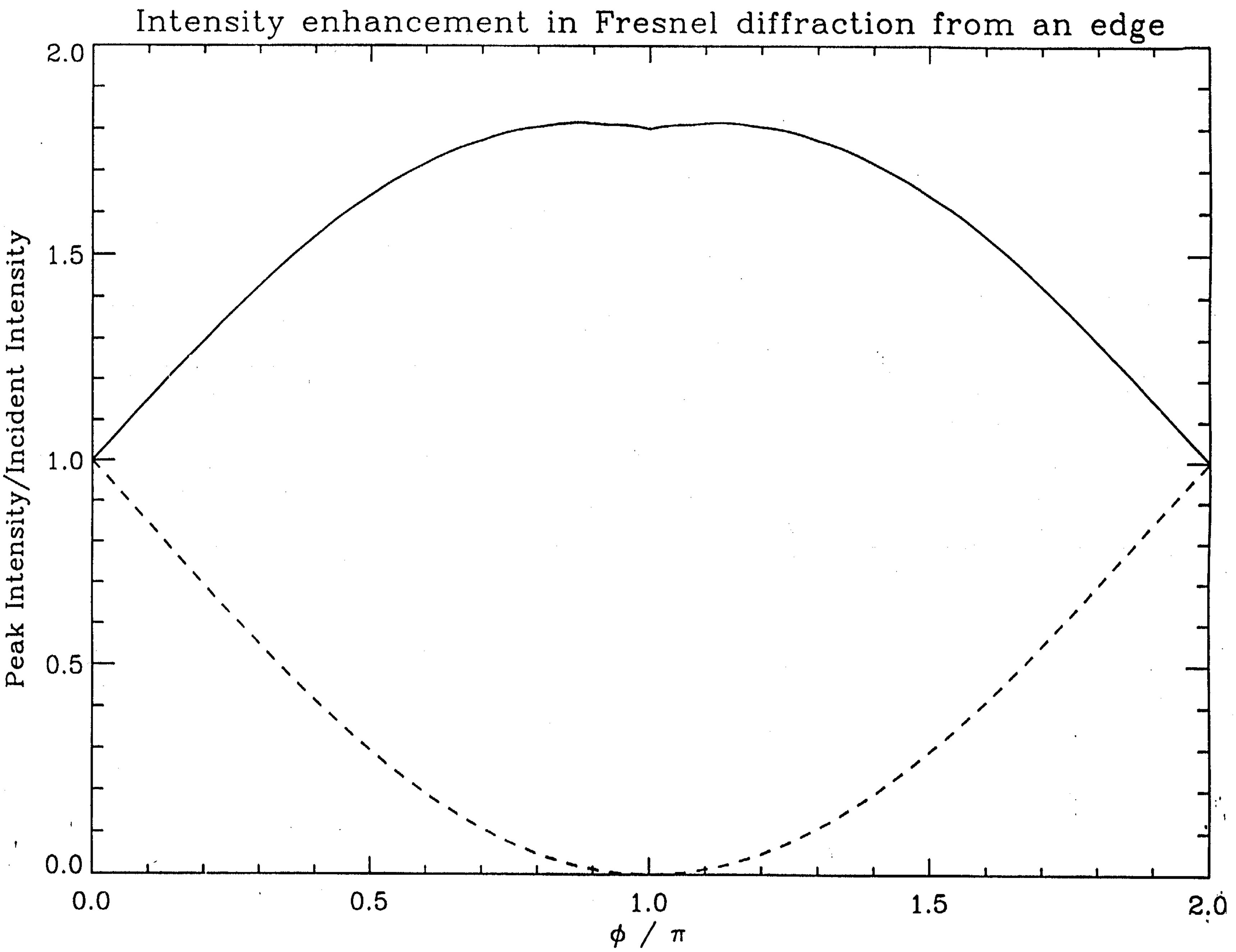
Intensity enhancement in Fresnel diffraction from an edge
Peak Intensity/Incident Intensity
2.0
1.5
1.0
0.5
0.0
0.0
0.5
1.0
1.5
2.0
$\phi$ / $\pi$

Figure 2

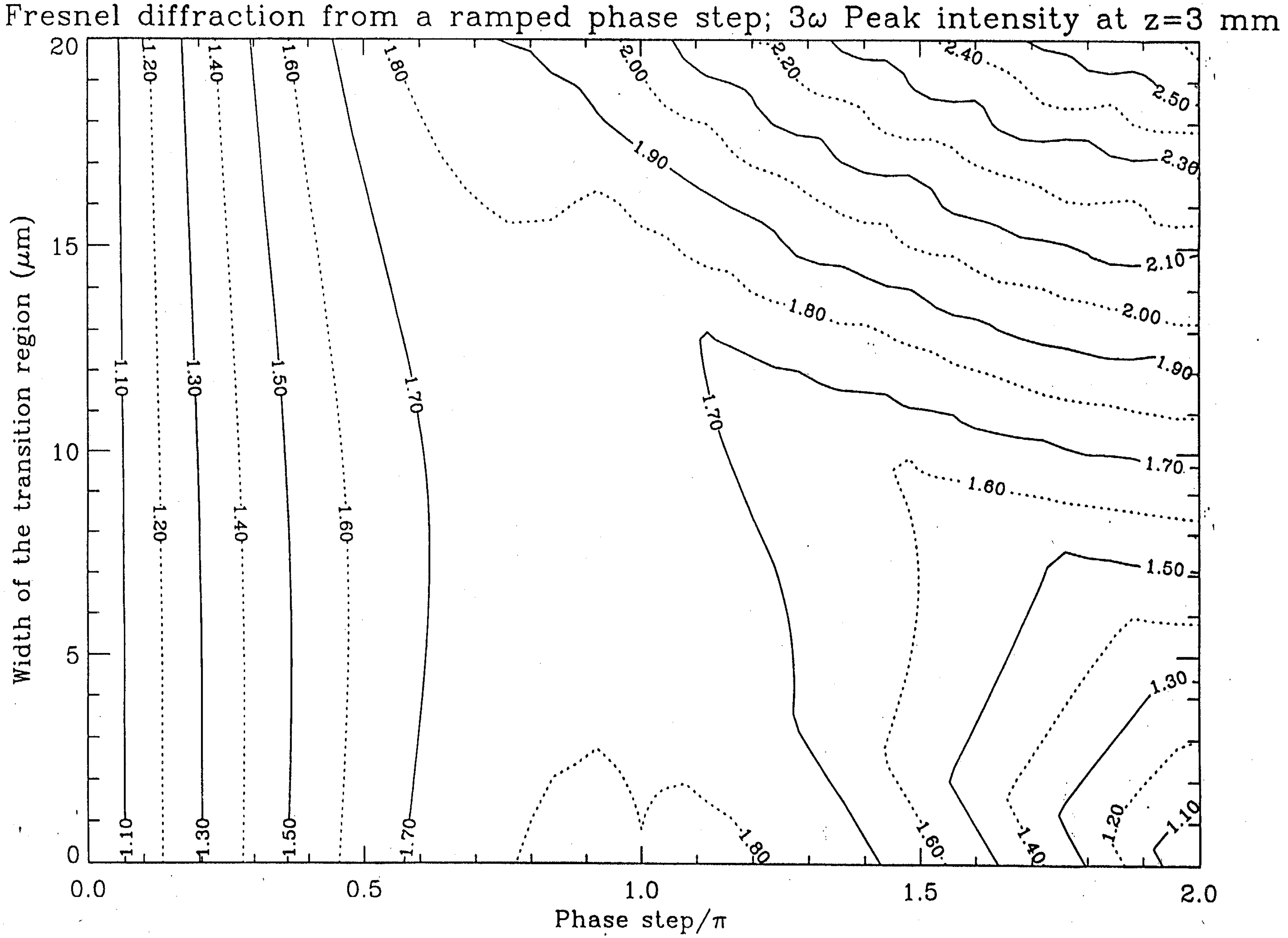

Fresnel diffraction from a ramped phase step; 3$\omega$ Peak intensity at $z=3$ mm

Figure 3

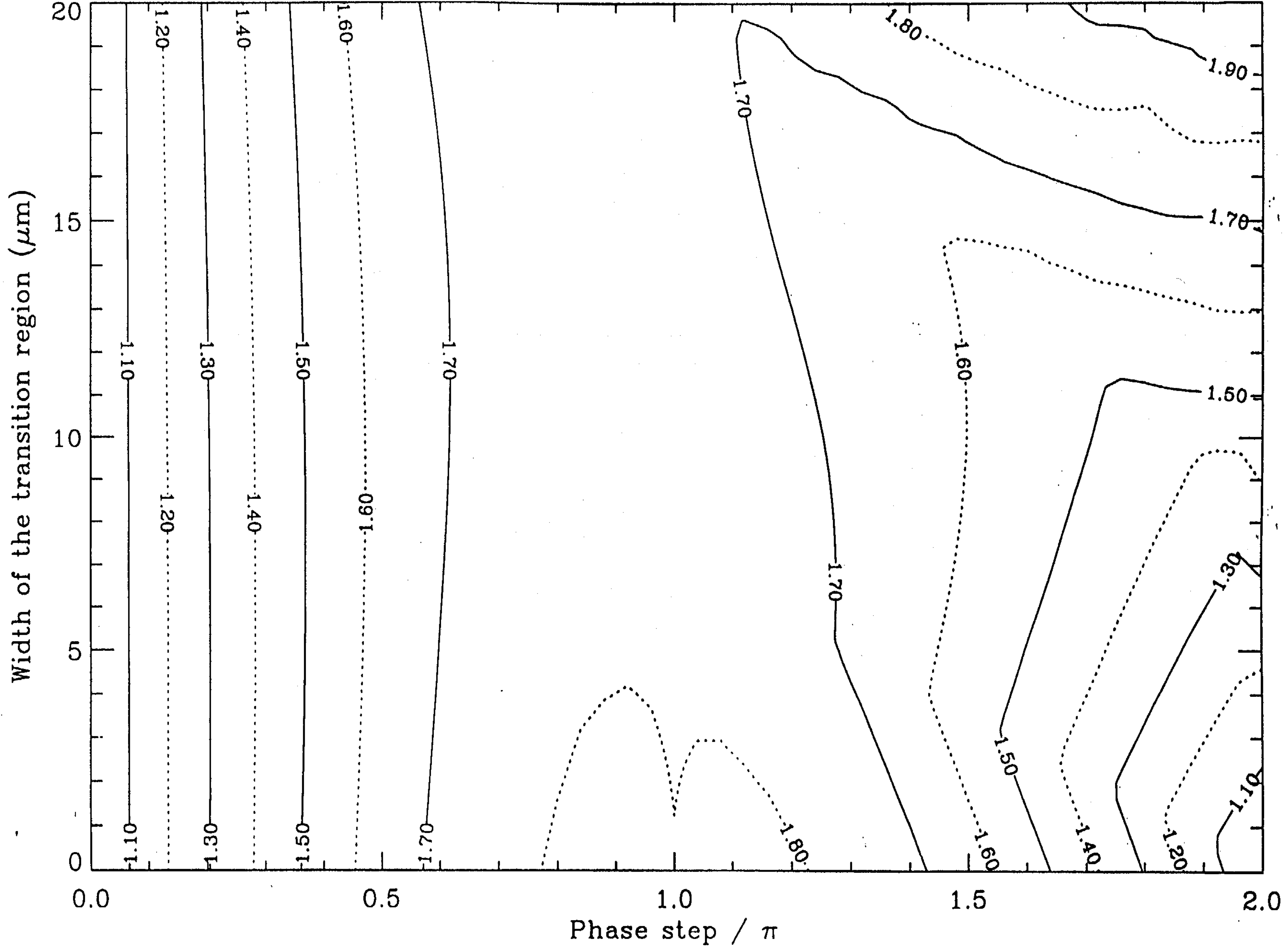
Fresnel diffraction from a ramped phase step; 3ω Peak intensity at z=7 mm

Figure 4

Fresnel diffraction from a ramped phase step; 3ω Peak intensity at z=1 cm

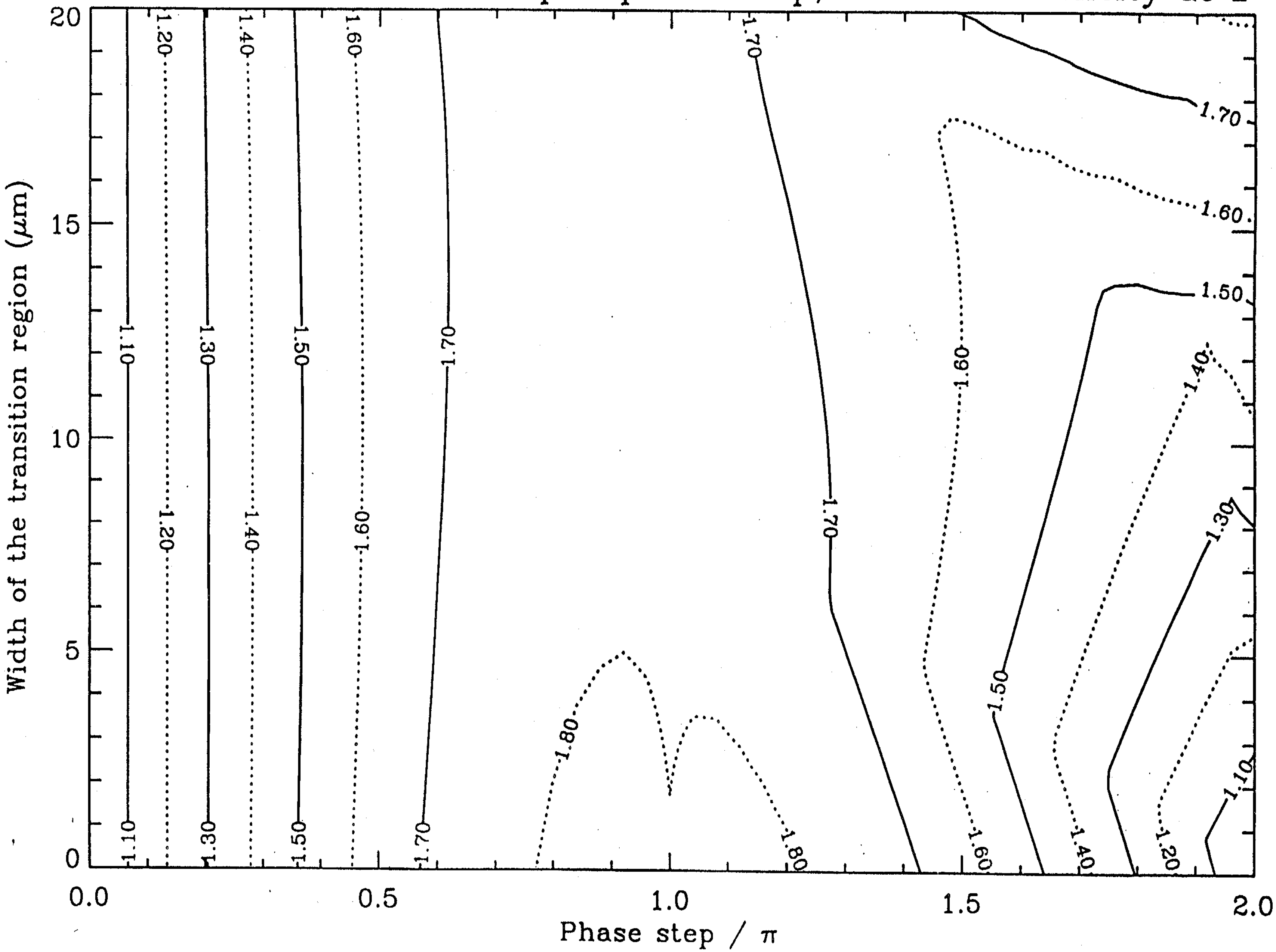

Figure 5

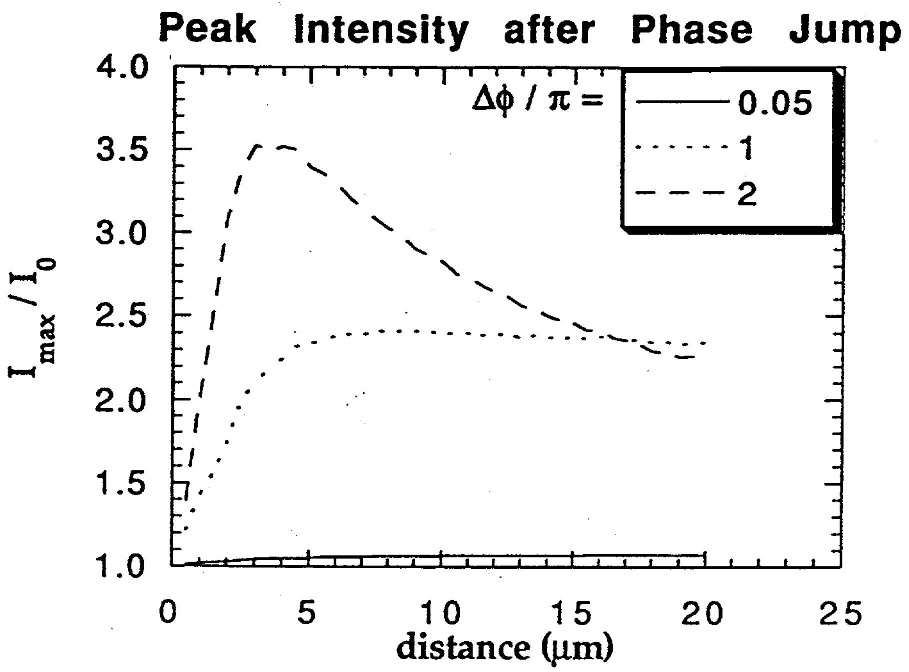
Peak Intensity after Phase Jump
Δφ / π =
0.05
1
2
$I_{max} / I_0$
4.0
3.5
3.0
2.5
2.0
1.5
1.0
0
5
10
15
20
25
distance (μm)

Figure 6

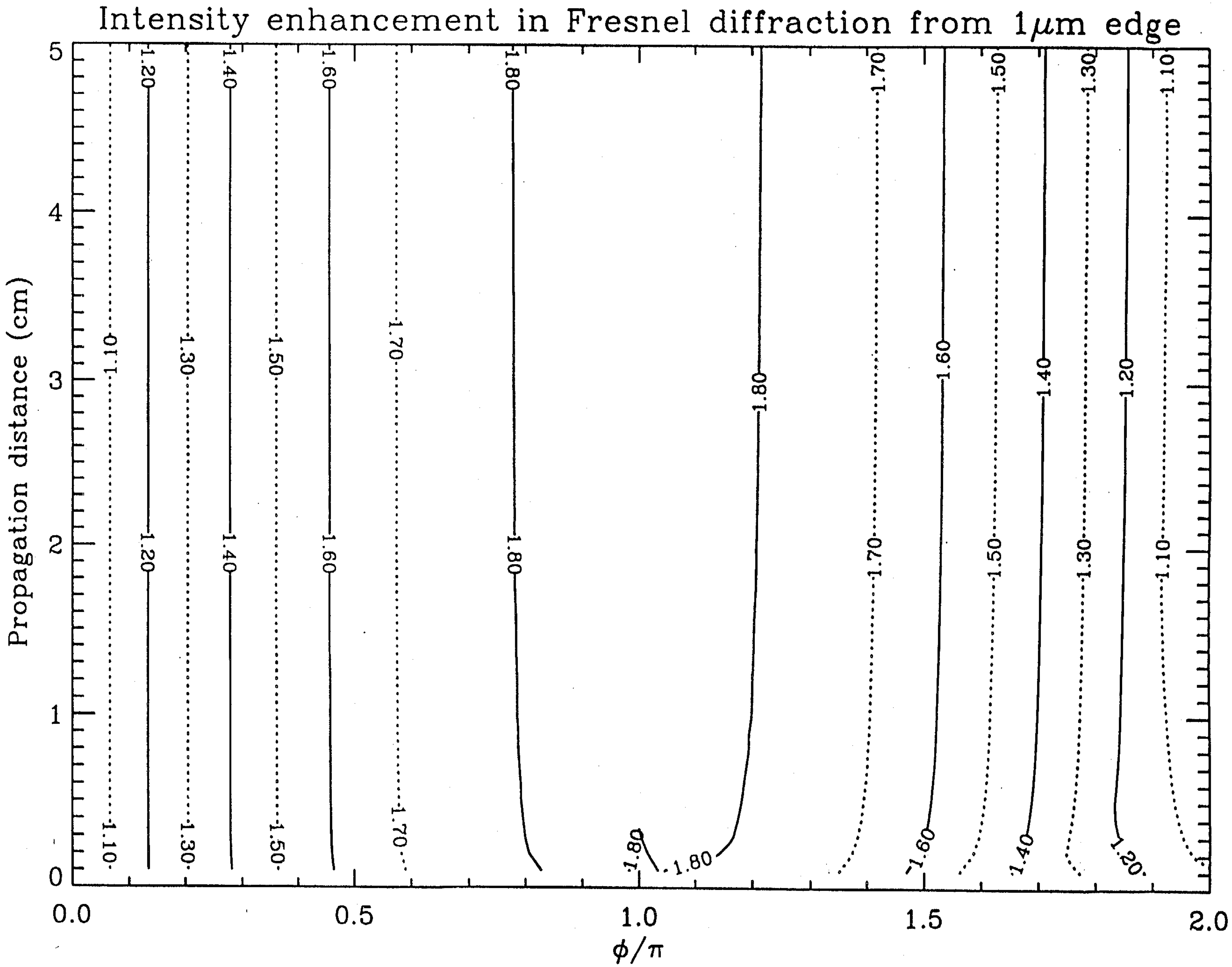
Intensity enhancement in Fresnel diffraction from 1$\mu$m edge
Propagation distance (cm)
$\phi/\pi$
0.0
0.5
1.0
1.5
2.0
0
1
2
3
4
5
1.10
1.20
1.30
1.40
1.50
1.60
1.70
1.80

Figure 7

# Kinoform phase plates for focal plane irradiance profile control

S. N. Dixit, J. K. Lawson, K. R. Manes, and H. T. Powell
*Lawrence Livermore National Laboratory, Livermore, Californina 94550*

K. A. Nugent
*School of Physics, University of Melbourne, Parkville, VIC 3052, Australia*

Received June 29, 1993

A versatile, rapidly convergent, iterative algorithm is presented for the construction of kinoform phase plates for tailoring the far-field intensity distribution of laser beams. The method consists of repeated Fourier transforming between the near-field and the far-field planes with constraints imposed in each plane. For application to inertial confinement fusion, the converged far-field pattern contains more than 95% of the incident energy inside a desired region and is relatively insensitive to beam aberrations.

In recent years it has become widely accepted that spatially and temporally smoothed laser beams are essential for suppressing the hydrodynamic and plasma instabilities in laser-driven inertial confinement fusion (ICF) targets.[1] Spatial smoothing, in which the beam is broken up into a fine-scale spatial structure that the target can potentially smooth by thermal conduction, is usually achieved by the use of random phase plates[2] (RPP's). RPP's used in many of the high-power ICF laser systems consist of regular layouts of square, rectangular, or hexagonal phase plate elements that impose either a 0 or a $\pi$ phase shift, chosen randomly for each RPP element. The far-field (FF) intensity pattern of such RPP's consists of a smooth overall envelope characteristic of the FF pattern of a single phase plate element (essentially an Airy pattern) and a superimposed speckle pattern resulting from the interference of light diffracted by various phase plate elements. Although such binary phase plates are easy to fabricate[3] and widely used, they offer little flexibility in tailoring the FF irradiance profile and increasing the energy content in the central maximum beyond the 84% predicted for an Airy pattern to the first zero.[4] In large fusion laser systems a 15% loss of the incident energy is quite significant, because it would correspondingly increase the cost of the entire laser system for delivering a fixed amount of energy to the target. Additionally, the scattered light could produce unwanted effects at the target. Thus it is highly desirable to tailor the beam profile on target to concentrate its energy content.

Qualitatively, the principal reason for large-angle diffraction from an RPP (which leads to the 15% energy loss) is the existence of abrupt phase boundaries. A more smoothly varying phase distribution would reduce the amount of large-angle scattering and hence increase the energy content in the central region. The question of designing a continuous phase screen can then be posed as: Is it possible to construct a phase screen in the input plane that, for a given input intensity distribution, produces a desired FF intensity distribution? This problem is somewhat similar to the well-known phase-retrieval problem of trying to deduce the phase of a field from its diffracted intensity distribution.[5]

In this Letter we present an iterative algorithm (similar to that used in phase-retrieval problems[5]) for systematically constructing continuously varying near-field (NF) phase screens for producing arbitrary focal plane irradiance distributions.[6] We refer to such phase screens as kinoform phase plates (KPP's). Numerical simulations indicate that the method is robust and rapidly convergent and that one can produce FF intensity profiles that contain greater than 95% of the incident energy in a desired central region. The KPP solution is observed to be relatively insensitive to the detailed phase distribution of the input beam, provided that the extent of the FF spot is substantially larger than that in the absence of KPP's. This robustness makes KPP's highly desirable for tailoring the FF irradiance profiles for ICF applications.

Several groups[7] have developed a lenslet array approach for generating smooth profiles by overlapping NF segments of the beam on target. Although it is useful, the lenslet approach does not offer the flexibility of generating arbitrary intensity profiles. Moreover, the optimum overlap plane has a limited depth of field compared with that of a KPP, which produces the desired profile in the FF.

For an illustration of the iterative algorithm, consider the focal plane characteristics of the light passing through a KPP and a focusing lens placed adjacent to it. The NF amplitude $E_{\mathrm{NF}}(x', y')$ and the FF amplitude $E_{\mathrm{FF}}(x, y)$ (both complex) are related to each other through the Fourier transform[3]

$$E_{\mathrm{FF}}(\nu_x, \nu_y) = -\frac{i}{\lambda f}\int_{\text{input aperture}} \mathrm{d}x'\,\mathrm{d}y' \times \exp\left[-i\frac{2\pi}{\lambda f}(xx' + yy')\right] E_{\mathrm{NF}}(x', y') \exp[i\phi(x', y')], \quad (1)$$

where $\nu_x = x/\lambda f$ and $\nu_y = y/\lambda f$ relate the FF distances to the Fourier frequencies and $\phi(x', y')$ denotes the phase introduced by the KPP. The KPP design problem then amounts to constructing a NF phase

0146-9592/94/060417-03$6.00/0

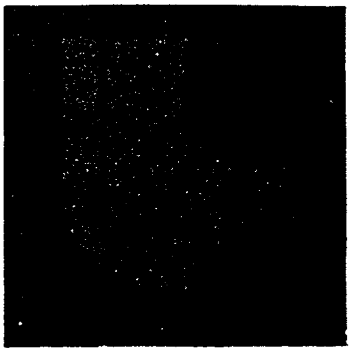

Fig. 1. Example of a complex FF intensity profile that can be produced by a suitably generated phase screen by use of the iterative algorithm described in this Letter.

screen $\phi(x',y')$ that produces the FF intensity profile $|E_{\mathrm{FF}}|^2$ given the NF intensity profile $|E_{\mathrm{NF}}|^2$. Note that no constraints are placed on the FF phase. This arbitrariness in the FF phase allows us to construct iteratively the phase screen $\phi(x',y')$.

The algorithm begins with the NF amplitude given by the square root of NF intensity and a random phase screen. Fourier transforming this complex amplitude leads to an amplitude- and phase-modulated FF distribution. At this point, a constraint is applied to the FF amplitude, leaving the phase unchanged. Inverse Fourier transforming this complex field gives a NF distribution that has both amplitude and phase modulations. The NF amplitude is then constrained to match the input intensity distribution while leaving the phase unchanged. The procedure is repeated again by Fourier transforming to the FF, etc. The iteration loop is repeated until an acceptable convergence is achieved in the FF.

The choice of the FF constraint is dictated by the specific problem under investigation. For ICF applications one is interested primarily in concentrating the energy within a desired region in the FF and not in the detailed distribution of intensity inside this region. Thus one can simply multiply (filter) the FF intensity with an appropriate weighting function. We find that the converged focal profile in this case is speckly in the region of interest. This is tolerable for ICF applications because the speckle can be smoothed by the plasma or by additional temporal smoothing techniques.[8] If a replacement constraint similar to that used in the NF is instead used in the FF, the converged FF intensity profile is nearly flat-topped with some residual fluctuations. However, addition of a realistic level of beam aberrations for ICF lasers again causes the FF intensity statistics to become a speckle pattern, although the overall envelope is maintained. For illustration, we focus here on the multiplicative constraint, deferring a more comprehensive discussion to a future publication.

We have numerically implemented the iterative algorithm to construct phase screens to tailor the far-field irradiance profiles. These simulations were carried out by fast-Fourier-transform techniques on a 512 × 512 grid. The input plane intensity profile is defined to be a fourth-order super-Gaussian,

$$I_{\mathrm{NF}}(x,y) = |E_{\mathrm{NF}}|^2 = \exp\{-[(x^2+y^2)/r_0{}^2]^4\}, \qquad (2)$$

where $r_0$ is the input beam radius. The diameter of the NF intensity profile was chosen to fill 70% of the grid. If we choose $r_0 = 35$ cm (Nova beam size), then the input grid spans 100 cm. This implies, with $f = 300$ cm and $\lambda = 0.527$ $\mu$m, a focal plane spatial resolution of 1.58 $\mu$m and a FF spatial extent of ~800 $\mu$m. The FF intensity weighting function is also chosen to be a fourth-power super-Gaussian similar to that in Eq. (2) with $r_f$ (instead of $r_0$) denoting the FF beam radius. In the numerical simulations presented here, we chose $r_f = 300$ $\mu$m. In general, one could use any reasonable integrable NF and FF profiles within the limits of diffraction, and the method would work adequately. We have successfully tested the algorithm by generating complex FF profiles as the logo of the Lawrence Livermore Laboratory, as shown in Fig. 1 for illustrative purposes.

Figure 2(a) shows the FF intensity distribution obtained after 50 iterations. The overall shape of the FF profile is well contained inside the 600-$\mu$m-diameter circle. The detailed FF intensity distribution resembles a speckle pattern with 100% intensity modulations. The fraction of the incident energy contained inside a circle of a given radius is plotted in Fig. 3 as a function of that radius for successive iterations. The improvement of the energy concentration with each iteration is clear. We see that the dominant part of the convergence is achieved after the first few (five or so) iterations and that the convergence improves extremely slowly thereafter. After

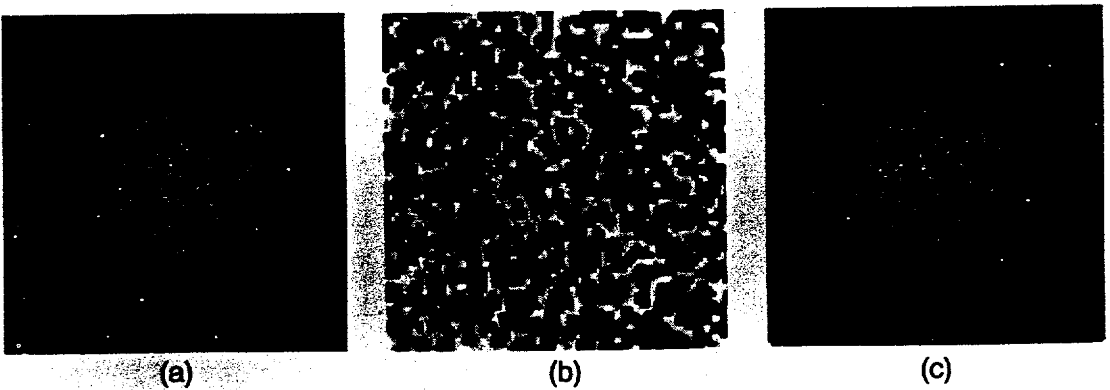

(a) (b) (c)

Fig. 2. (a) FF intensity distribution obtained after 50 iterations. The spatial extent of the image is 800 $\mu$m × 800 $\mu$m. (b) A portion of the NF kinoform phase screen. The gray scale spans from $-\pi$ (black) to $\pi$ (white). The spatial extent of the image is 15 cm × 15 cm. (c) The same as (a) but including the input beam phase aberrations.

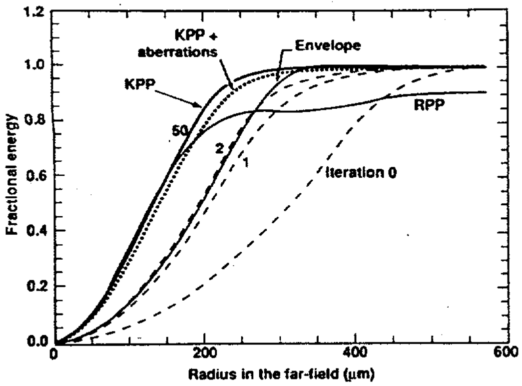

Fig. 3. FF energy content as a function of the FF radius (see text for a description of the various curves).

the 50 iterations considered in this example, the 600-$\mu$m-diameter circle contains greater than 95% of the incident energy. This is a significant improvement in the energy content over a binary RPP, in which the element size is chosen such that the size of the central maximum (to the first zero) is equal to the size of the FF super-Gaussian profile ($r_f$) (curve labeled RPP in Fig. 3). It is also interesting to note that the energy concentration near the center is better than that for the envelope; a consequence of the multiplicative constraint that leaves the central portion of the FF unaffected. On the other hand, a replacement constraint produces a FF pattern whose energy content closely follows the curve labeled Envelope.

The NF phase screen obtained after the iterative optimization [a portion of which is shown in Fig. 2(b)] shows a rippled structure. The characteristic scale size is ~5 mm, corresponding to the 600-$\mu$m FF spot size. This phase distribution is fairly smooth, except for discrete jumps of approximately $2\pi$ that result from the determination of the phase by the numerical arctangent function [which is limited to the range $(-\pi, \pi)$]. Techniques for two-dimensional unwrapping of the phase are under investigation.

We now discuss the use of the KPP's on aberrated lasers such as the Nova. Since the input electric-field amplitude will be a product of the KPP phase screen and the Nova laser beam amplitude, the FF amplitude will be a convolution of the FF amplitudes for the KPP and the Nova beam separately (Schell's theorem[9]). Thus one can expect that, if the extent of the FF pattern produced by the KPP is much larger than that produced by the beam alone, the convolution should not significantly affect the overall FF shape. To investigate this issue, we have constructed a realistic model for Nova beam aberrations, which produces a FF spot approximately 150–200 $\mu$m wide, comparable with experimentally measured Nova FF spots. The FF irradiance profile produced by the KPP with such an aberrated beam is shown in Fig. 2(c). Comparing this with the FF profile in Fig. 2(a), we see that the beam aberrations change the details of the speckle and slightly broaden the FF spot. However, the energy content within it (curve labeled KPP + aberrations in Fig. 3) is not significantly altered. This is because the overall FF spot size is governed by a local NF phase scale, whereas the fine-scale FF structure results from the long-scale NF phase variations. The requirement that the FF spot size without KPP be much smaller than that determined by the KPP alone ensures that the beam has constant phase over the characteristic KPP phase scale lengths.

In summary, we have presented a rapidly convergent iterative procedure with which to construct kinoform phase plates for producing desired FF profiles with efficient energy concentration. Numerical simulations indicate that the resulting far-field profile contains greater than 95% of the incident energy within the desired region. The beam aberrations have a small effect on the performance of KPP's as long as the far-field spot produced by the KPP's is significantly larger than that produced by the beam aberrations alone. We are currently fabricating KPP's in high-optical-damage-threshold materials.

We acknowledge many useful discussion with D. Eimerl, R. W. Hellwarth, M. A. Henesian, and J. B. Trenholme and thank Paul Wegner for providing us with the Nova beam aberrations model. Research done at Lawrence Livermore National Laboratory was performed under the auspices of the U.S. Department of Energy under contract W-7405-Eng-48.

## References

1. J. D. Lindl, R. L. McCrory, and E. M. Campbell, Phys. Today **45** (9), 32 (1992).
2. Y. Kato, K. Mima, N. Miyanaga, S. Arinaga, Y. Kitagawa, M. Nakatsuka, and C. Yamanaka, Phys. Rev. Lett. **53**, 1057 (1984).
3. S. N. Dixit, I. M. Thomas, B. W. Woods, A. J. Morgan, M. A. Henesian, P. J. Wegner, and H. T. Powell, Appl. Opt. **32**, 2543 (1993), and references therein.
4. M. Born and E. Wolf, *Principles of Optics*, 6th ed. (Pergamon, New York, 1980), Chap. 8, p. 393.
5. See, for example, J. R. Feinup, Appl. Opt. **21**, 2758 (1982).
6. A preliminary account of this research was reported by J. K. Lawson, S. N. Dixit, D. Eimerl, M. A. Henesian, K. R. Manes, A. J. Morgan, H. T. Powell, I. M. Thomas, J. B. Trenholme, and B. W. Woods, Proc. Soc. Photo-Opt. Instrum. Eng. **1870**, 88 (1993).
7. X. Deng, X. Liang, Z. Chen, W. Yu, and R. Ma, Appl. Opt. **25**, 377 (1986); T. Jitsuno, N. Nishi, K. Tsubakimoto, M. Nakatsuka, K. Nishihara, and S. Nakai in *Conference on Lasers and Electro-Optics*, Vol. 12 of 1992 OSA Technical Digest Series (Optical Society of America, Washington, D.C., 1992), paper CThI2; C. N. Danson, Rutherford Appleton Laboratory, Didcot, Oxon. OX11 0QX, UK (personal communication, 1993).
8. See, for example, H. T. Powell, S. N. Dixit, and M. A. Henesian, LLNL ICF Quarterly Rep. UCRL-LR-105821-91-1 (Lawrence Livermore National Laboratory, Livermore, Calif., 1990), pp. 28–38; S. Skupsky, R. W. Short, T. Kessler, R. S. Craxton, S. Letzring, and J. M. Soures, J. Appl. Phys. **66**, 3456 (1989).
9. J. W. Goodman, *Statistical Optics* (Wiley, New York, 1985), Chap. 5, p. 225.

IV

# Fused silica kinoform phase plates for generation of uniform focal plane irradiance profiles

S. N. Dixit, I. M. Thomas, M. Rushford, R. Merrill, M. D. Perry and
H. T. Powell

Lawrence Livermore National Laboratory, Livermore, California 94550, USA

## Abstract

We have fabricated 12-cm diameter, 16-level kinoform phase plates in fused silica using lithographic techniques and wet etching in a buffered hydrofluoric acid solution. The experimentally measured far-field intensity pattern under 514-nm laser illumination displays the desired top-hat envelope with superimposed speckle and contains approximately 90% of the incident energy inside the top-hat envelope.

It is now widely recognized that spatial and temporal beam smoothing is essential for suppressing laser-plasma instabilities and for uniformly irradiating inertial confinement fusion (ICF) targets [1]. For ICF applications, it is often desirable to produce top-hat intensity profiles which contain as much of the incident energy as possible. Binary random phase plates (RPPs) have been widely used [2,3] for producing homogeneous intensity profiles in the focal plane with a superimposed fine-scale speckle. The speckle is usually 'smoothed' (in terms of how the target responds to it in a space- and/or time-averaged sense) either by the plasma (conduction smoothing) [1] and/or by externally applied temporal smoothing [4]. As has been discussed elsewhere [3], the RPP far-field envelope resembles an Airy pattern and contains only about 82% of the incident energy within the central spot. A refractive lenslet array [5] and very recently, a binary, diffractive phase zone plate array [6] have been proposed for producing top-hat irradiance profiles with increased energy efficiency at the target. The depth of field of the uniform profiles produced by these methods is very limited as the top-hat profiles are obtained by working in a specific quasi-far-field plane. In a recent paper [7], we have presented an iterative algorithm for constructing continuous contour phase screens (called kinoform phase plates or KPPs) which can produce arbitrary-shaped irradiance profiles in the focal plane and contain most of the incident energy inside the desired region. Our simulations have shown that it should be possible to produce top-hat supergaussian irradiance profiles in the far-field that contain more that 95% of the incident energy inside the central spot.

In this letter we report on the optical performance of a 16-level, 12-cm diameter aperture fused silica KPP fabricated using lithographic techniques and wet etching of fused silica in a buffered hydrofluoric acid solution. Since the KPP phase profile is etched directly into fused silica, the finished product has a high laser damage threshold at ultraviolet wavelengths (~ 18 J/cm$^2$ for 3-ns pulses at 351 nm). The experimentally measured far-field intensity pattern displays the desired top-hat envelope and has superimposed speckle on it. The far-field contains approximately 90% of the incident energy inside the designed 640 μm region. This is a significant improvement over the binary RPP's in terms of the far-field profile control and energy concentration. Sources contributing to the energy loss are discussed.

Using the iterative algorithm described previously [7], we designed the KPP to produce a 640 μm diameter 8-th power super-Gaussian intensity profile in the focal plane when irradiated with 527-nm light and focused with a 3-m focal length lens. The computer-generated phase screen consists of continuously varying phase regions as well as ~ $2\pi$ phase discontinuities. The pixel size was chosen to be 305 μm square and the KPP spanned 410 pixels in diameter so that the KPP size was about 12.5 cm in diameter. The square pixels on the KPP lead to a large-scale two-dimensional sinc$^2$ envelope pattern in the far-field. The desired top-hat profile is superimposed on this envelope pattern. For a 305 μm square aperture of a single pixel in our case, the first zero of the sinc$^2$ envelope occurs at ~ 5 mm from the center. We have verified theoretically that less than 1% of the incident energy is lost in the secondary maxima.

The KPP was fabricated using lithographic techniques and wet etching of fused silica in a buffered hydrofluoric acid solution. Here $2^N$ phase levels can be fabricated using N binary amplitude masks and varying the etch times with each mask. We quantized the computer generated KPP phase screen to

16 phase levels so that they can be fabricated using four binary amplitude masks. Our calculations indicate that for the present pixel size, the 16-level quantization of the phase screen leads to ~ 1% energy loss outside the desired region compared to a fully continuous phase screen. A $2\pi$ relative phase delay corresponds to an etch depth of $t = \lambda/(n-1)$ where n is the refractive index at the operating wavelength $\lambda$. In the multiple binary mask approach, etching following exposure through mask 1 is for a depth t/2, that following mask 2 is for a depth t/4, the next one for t/8 and so on. At the end of the procedure one ends up with $2^N$ phase levels ( 0 to $2^N$-1) with a maximum etch depth of $t\,(1-1/2^N)$ . Since the present KPP was fabricated for use at 527 nm, t = 1146 nm (n = 1.46 for fused silica), and the smallest etch depth was 72 nm.

We fabricated the 16-level KPP through a sequence of steps consisting of: photoresist coating, exposing through the appropriate binary mask, developing of the resist, and etching of unprotected areas on the substrate for the required etch depth. Approximately 120 nm of chrome was deposited on 1.5-cm thick, 15-cm diameter fused silica substrates prior to the KPP fabrication. We cleaned the substrate with a UV/ozone treatment and used an adhesion promoter, hexamethyldisilizane (HMDS), to ensure a good bond between the substrate and the photoresist and to avoid undercutting and peeling during the subsequent etching. Approximately 2 µm thick layer of photoresist (Shipley 1400) was spin coated onto the substrate and fully exposed through the mask using an extended white light source. The binary amplitude masks for each exposure stage were prepared using a Gerber photo-plotter on acetate based photographic film. The etching was done in a constant temperature, buffered hydrofluoric acid solution (1% HF + 15% NH4F) with the longest etch time of 28 minutes. A similar procedure has been recently reported for fabricating a 16 level diffractive optical element for intensity shaping a laser cavity mode [8].

Accurate overlay of masks is crucial to obtaining sharp edges between the pixels on the KPP. Wider edges lead to large-angle scattering and hence to a reduction in the amount of energy contained inside the central top-hat profile. We aligned the masks using three alignment fiducials written on the film at the edge of the KPP pattern. The fiducials on masks 2, 3 and 4 were aligned, prior to exposure, with those initially patterned on the substrate from mask 1. We found that the masks made on acetate film lead to considerable overlay inaccuracy across the KPP aperture because of the flexibility of the film. We are currently investigating minimizing this error by producing the binary masks on rigid glass substrates. Figure (1a) shows a white-light interferogram of the KPP which exhibits various phase levels as grey scales. A magnified view of a small section of the KPP (Figure (1b)) shows the pixelated nature of the KPP phase screen. High resolution microscope pictures of the edges indicate that some of the edges were very sharp (better than 2 μm) while others were very broad (~ 20 μm). Based on relative area, we estimate about 1-2% loss in energy efficiency due to wide-angle scattering resulting from these edges. The step heights of different phase levels were measured on four calibration strips fabricated at the edge of the KPP using a Dektak stylus profilometer. The ratio of the average of the four step height measurements to the expected values for a KPP for use at 527 nm (j72 nm j=0,1..15) are 1.0 (normalization), 1.054, 1.111, 1.054, 1.028, 1.025, 1.006, 1.005, 0.990, 1.002, 0.996, 0.999, 1.014, 0.995, 1.006 and 0.997. The deviations in the measured step heights were on the order of ± 10 nm.

We evaluated the optical performance of the KPP by measuring the far-field intensity profile and its energy content. The monochromatic output of an argon-ion laser at 514 nm was collimated, passed through the KPP and focused using a 3-m focal length lens. The far-field image was recorded on film, digitized using a photodensitometer and the digitized image was processed to calculate the irradiance distribution. One such focal plane intensity profile as recorded on the film is shown in figure 2a while a line-scan across the center of a processed image is shown in figure 2b. Although the far-field image has a relatively coarse modulation for this small KPP, the ~ 640 μm diameter top-hat nature of the profile is evident. In figure 2c we show line scans through the calculated far-field patterns using the measured average step heights given above and for illuminating the KPP with 514 and 527 nm coherent light. We see that, illuminating the KPP with a coherent 514 nm laser is predicted to give a small (~ 4:1) coherent spike at the center of the far-field image because the KPP was designed for use at 527 nm. The rest of the far-field pattern and the energy content show insignificant differences between the two wavelengths. On the other hand, the experimental data (figure 2b) does not show any significant coherent spike at the far-field center. We believe this is probably due to imperfections in the actual step heights across the KPP as well as due to optical aberrations in the beam. The measured intensity pattern has an overlaid speckle of comparable modulation depth to that predicted. The details of the speckle in the two cases, however, would be expected to be different since even a small amount of aberrations would alter the speckle distribution in the far-field.

In addition to the desired top-hat profile, we also observed a halo around the central pattern and the diffraction pattern of the individual 305 µm pixels extending to several orders in the horizontal and the vertical directions. These features are at much lower intensities compared to the desired central spot and are, therefore, not visible in figure 2. The features due to diffraction from a pixel can be eliminated by fabricating a continuously varying phase screen (as opposed to the pixelated one fabricated here). The halo can also be minimized in a discrete KPP by sharpening the pixel edges. Fabrication of KPPs with finer edge width is currently underway.

The energy concentration in the focal plane was determined by measuring the energy passing through pinholes of differing sizes normalized to the total energy in a near-field plane following the KPP. This comparison removes the Fresnel reflection losses from the non-anti-reflection coated surfaces of the KPP. The measured energy concentration is compared with the calculated energy distribution in figure 3. The measured fractional energy values follow closely the ideal theoretical values but seem to be about 5% below them. We believe majority of this deviation is due to poor edge definition. Nevertheless, the 640 µm diameter region contains approximately 90% of the incident energy. This is a significant improvement over the binary RPP energy content of 82%.

In summary, we have fabricated a 16-level KPP on a 12-cm diameter aperture fused silica using lithographic techniques and wet chemical etching. The measured far-field intensity pattern displays the expected top-hat envelope and has a superimposed speckle on it. The far-field contains approximately 90% of the incident energy inside the designed 640 µm diameter region. This is a significant improvement over the binary RPP's in terms of the far-field profile control and energy concentration. We are currently working on improving the efficiency of the KPP and developing methods to scale up the technology for fabricating large aperture (65-cm diameter) KPP's for use on the Nova laser .

## Acknowledgments

We thank Professor J. R. Leger for valuable discussions during the course of our KPP development. This work was performed under the auspices of the U. S. Department of Energy by the Lawrence Livermore National Laboratory under contract W-7405-Eng-48.

## References

[1] J. D. Lindl, R. L. McCrory and E. M. Campbell, Physics Today 45 32 (1992)

[2] Y. Kato, K. Mima, N. Miyanaga, S. Arinaga, Y. Kitagawa, M. Nakatsuka and C. Yamanaka, Phys. Rev. Lett. 53 1057 (1984).

[3] S. N. Dixit, I. M. Thomas, B. W. Woods, A. J. Morgan, M. A. Henesian, P. J. Wegner and H. T. Powell, Appl. Opt. 32 2543 (1993) and references therein.

[4] See, for example, S. Skupsky, R. W. Short, T. Kessler, R. S. Craxton, S. Letzring and J. M. Soures, J. Appl. Phys. 66 3546 (1989).

[5] X. Deng, X. Liang, Z. Chen, W. Yu, and R. Ma, Appl. Opt. 25 377 (1986)

[6] R. M. Stevenson, M. J. Norman, T. H. Bett, D. A. Pepler, C. N. Danson and I. N. Ross, Opt. Lett. 19 363 (1994).

[7] S. N. Dixit, J. K. Lawson, K. R. Manes, H. T. Powell and K. A. Nugent, Opt. Lett 19 417 (1994).

[8] J. R. Leger, D. Chen and Z. Wang, Opt. Lett 19 108 (1994).

## Figure Captions

Figure 1 (a) White-light interferogram of the KPP. Various phase levels are displayed as different grey levels; (b) A magnified image of a section of the KPP. Pixel size on the KPP is 305 μm.

Figure 2. (a) Film image of the far-field intensity distribution produced by the KPP; (b) Horizontal line scan through the center of a far-field image such as the one shown in (a) following processing. The dashed line denotes the 8th power supergaussian envelope; (c) Horizontal line scan through the center of the calculated KPP far-field pattern for illumination with 527 nm (solid line) and 514 nm (dot-dashed line) coherent radiation. Note the slight change in the far-field spatial scale for 514 nm and 527 nm wavelengths. The dashed line againdenotes the 8th power supergaussian envelope (shown for 527 nm).

Figure 3. Energy concentration in the far-field produced by the KPP. Solid line denotes the calculated energy concentration and the points correspond to the measured normalized energy passing through various sized pinholes.

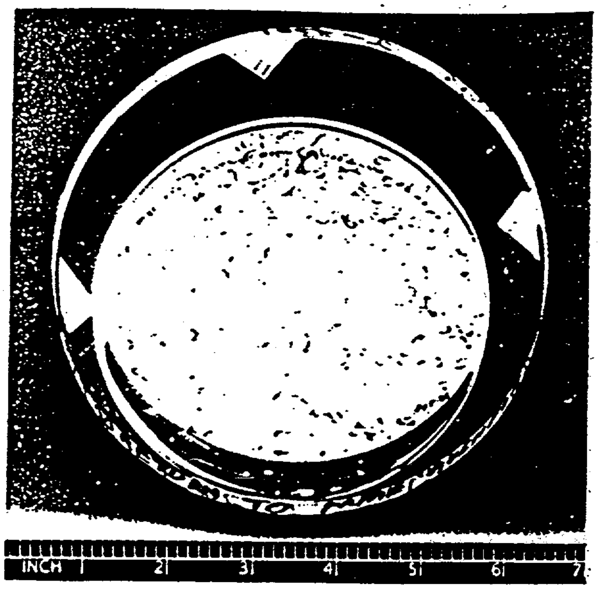

Fig 1a

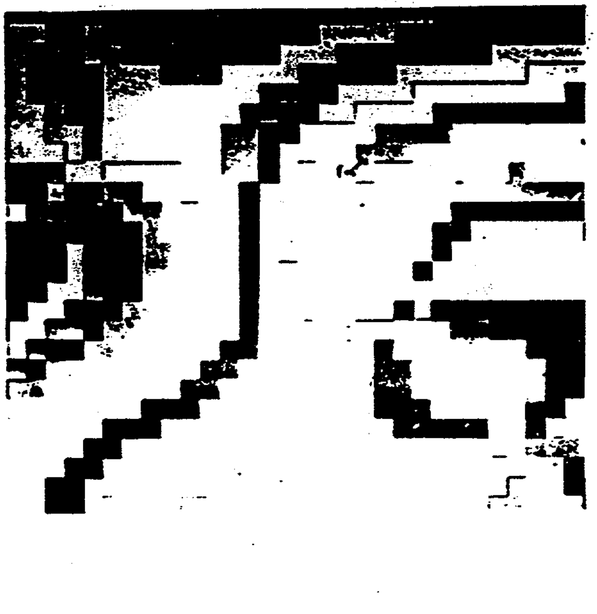

Fig 1b

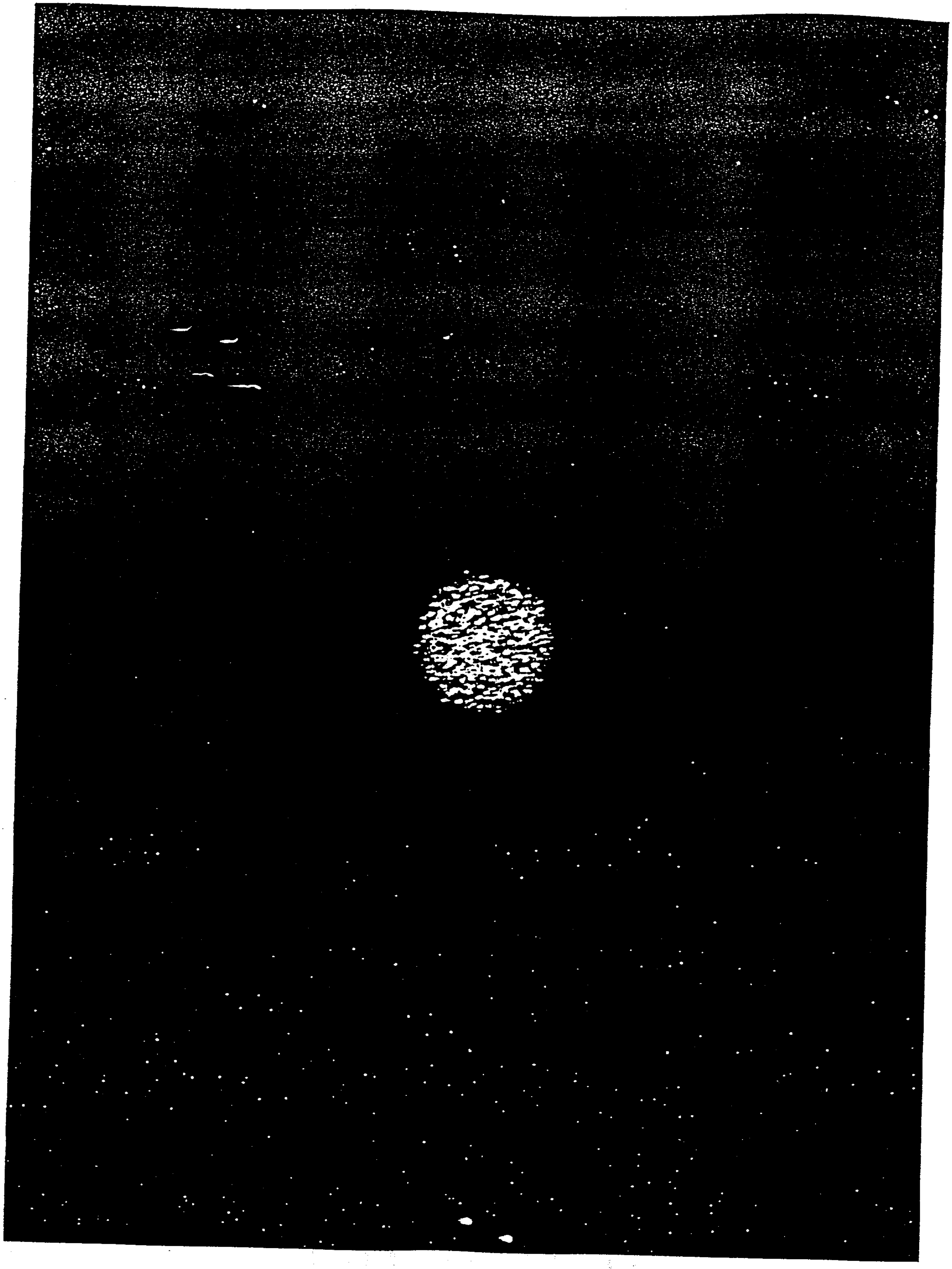

Fig 2a

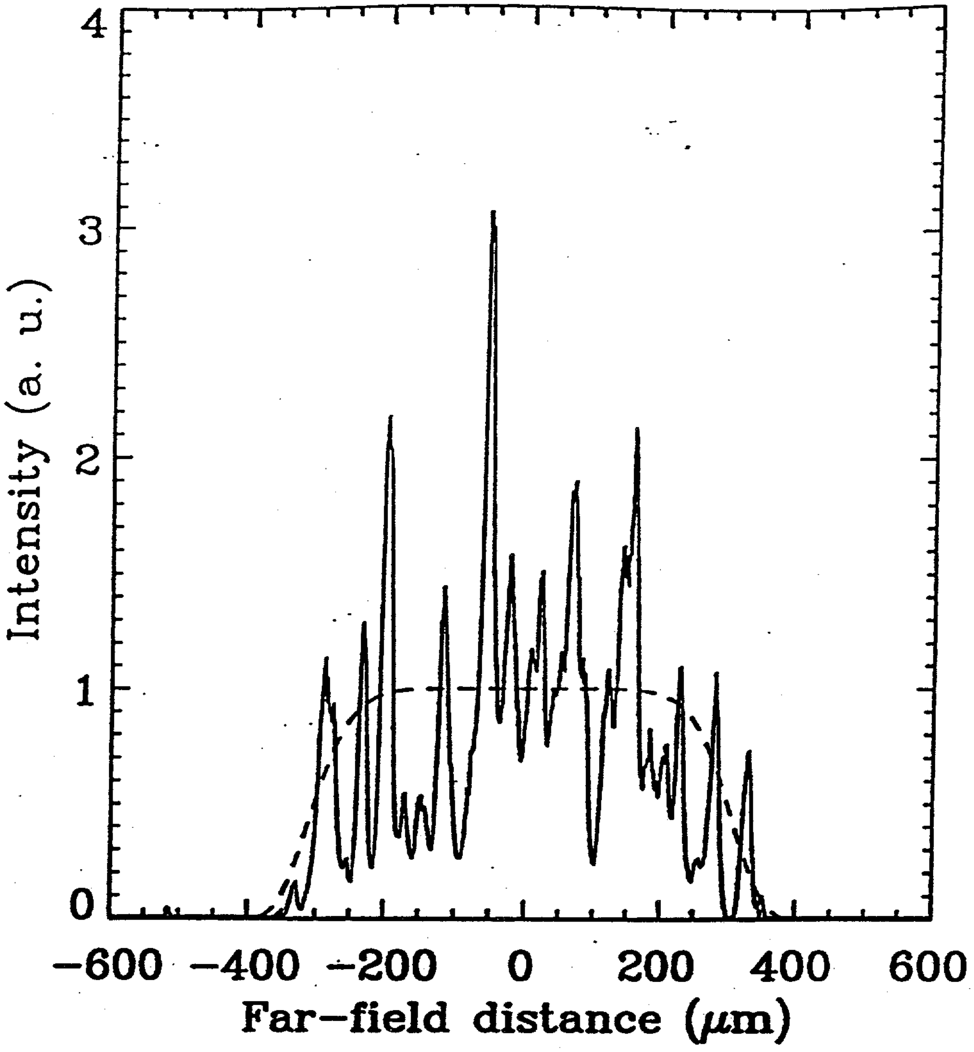
4
3
2
1
0
Intensity (a. u.)
−600
−400
−200
0
200
400
600
Far−field distance (μm)

Fig 2b

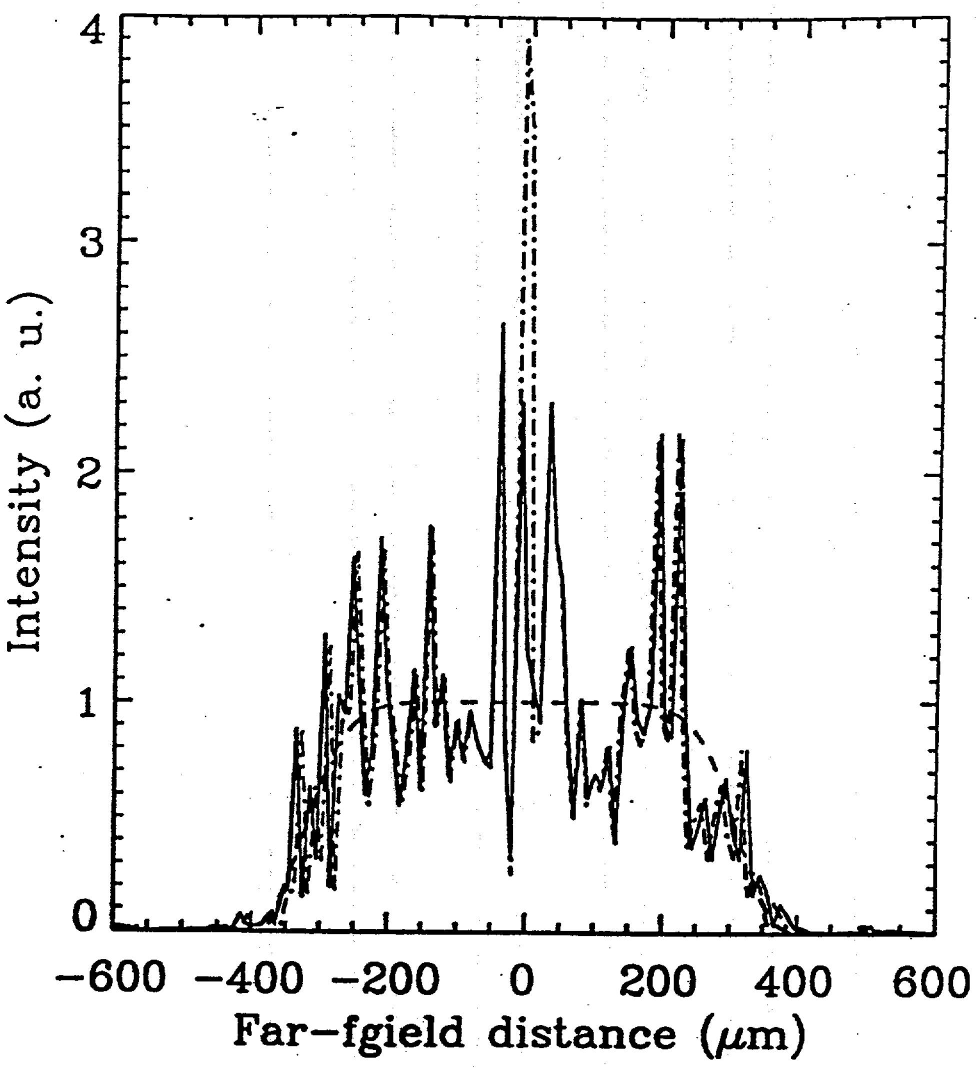
4
3
2
1
0
Intensity (a. u.)
−600
−400
−200
0
200
400
600
Far−fgield distance (μm)

Fig. 7a

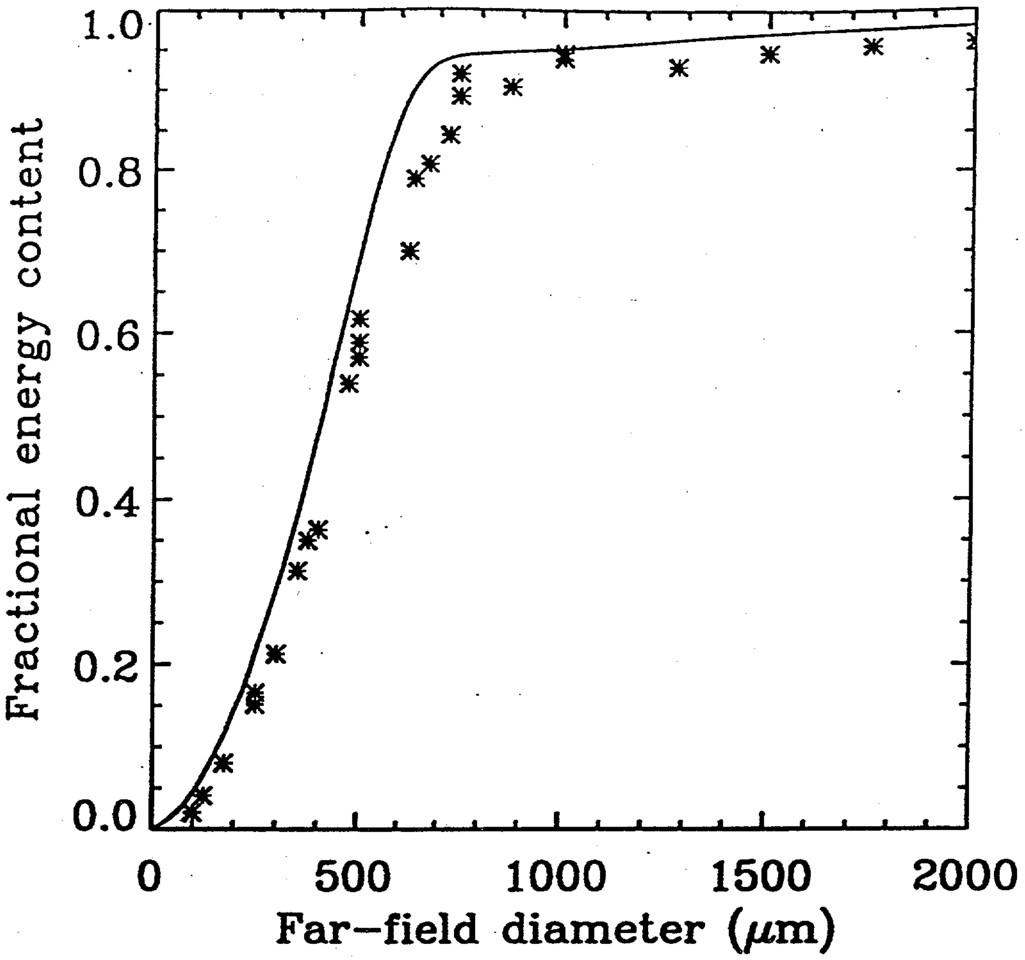

Fractional energy content
1.0
0.8
0.6
0.4
0.2
0.0
0
500
1000
1500
2000
Far–field diameter (μm)

Fig 3

# KINOFORM PHASE PLATES FOR TAILORING FOCAL PLANE INTENSITY PROFILES

*S. N. Dixit*
*I. M. Thomas*
*M. R. Rushford*
*R. Merrill*
*M. D. Perry*
*H. T. Powell*
*K. A. Nugent**

## Introduction

In recent years, it has become widely accepted that smooth laser beams are essential for controlling and possibly suppressing hydrodynamic and plasma instabilities in laser-driven inertial confinement fusion (ICF) systems.[1] In directly driven targets, hydrodynamic instabilities seeded by the nonuniformities in the laser beam can destroy the symmetry of the implosion. On the other hand, in indirectly driven targets, parametric instabilities in the plasma surrounding the capsule can lead to energy loss and redistribution due to scattering and thus affect the coupling efficiency and drive symmetry. Techniques developed for smoothing laser beams can be divided into two categories:

- Spatial smoothing—The beam is broken up into a fine-scale spatial structure that the target potentially can smooth by thermal conduction.
- Temporal smoothing—The fine-scale structure is changed rapidly in time, resulting in a beam with a smooth, time-averaged profile.

In each of these methods, the plasma has to "experience" smoothing through spatial and/or temporal averaging. Spatial smoothing is achieved by using random phase plates (RPPs)[2] or lenslet arrays,[3,4] whereas temporal smoothing is implemented by spectral dispersion (SSD),[5] induced spatial incoherence (ISI),[6] or amplified spontaneous emission (ASE)[7,8] techniques. In a previous issue of this *Quarterly*, we described beam smoothing on the Nova laser using RPPs and SSD.[9] Time-integrated smoothing levels of about 10% (rms intensity variations normalized to the average intensity) were achieved in averaging times of about 100 ps.

RPPs have been used in many high-power ICF laser systems for producing a more homogeneous focal plane irradiance. All RPPs used so far have consisted of square, rectangular, or hexagonal elements that impose either a zero or π phase shift at random locations on the beam. The far-field intensity pattern of such RPPs consists of an envelope characteristic of the far-field pattern of a single phase-plate element and a superimposed speckle pattern resulting from interference among the contributions of various phase-plate elements. The far-field envelope for square and hexagonal shapes is qualitatively similar to an Airy pattern, and it contains roughly 81 to 84% of the incident energy within the central maximum.[9,10] Although such regular-element, binary phase plates are easy to fabricate[11] and are widely used, they offer us little flexibility in tailoring the far-field irradiance profile and in increasing the energy content in the central maximum beyond the 84% predicted for a circular aperture. In high-power fusion laser systems, the remaining 15% or so of the incident energy lost due to diffraction would increase the cost of the laser system because the system would have to be run at higher energy levels in order to deliver the required amount of energy on target. Additionally, the scattered energy could also damage diagnostic equipment located near the target. Thus, it is desirable to tailor the far-field profile and also increase the energy content therein.

The principal reason for large-angle diffraction from an RPP (which leads to the 15% energy loss) is the existence of discrete phases and abrupt phase boundaries. A smoothly varying phase in the near field would reduce the amount of large-angle scattering and thus increase the energy content. Therefore, both the binary and regular phase-plate element assumptions must be relaxed.

Recently, we presented[12] a robust, rapidly convergent, iterative algorithm for constructing continuous-phase screens that can produce arbitrary-shaped irradiance profiles in the focal plane and contain most of the incident energy inside the desired region. We call such phase plates *kinoform phase plates* (KPPs). The

---

*School of Physics, University of Melbourne, Parkville, VIC 3052, Australia

iterative algorithm is similar to those used in phase-retrieval problems. Our simulations have shown that it should be possible to produce "top-hat" supergaussian irradiance profiles in the far field that contain more than 95% of the incident energy inside the central spot.

We also fabricated[13] such a KPP in a 12.5-cm-diam fused-silica substrate by means of lithographic techniques and wet-etching of fused silica in a buffered hydrofluoric acid solution. The KPP was designed by using the iterative algorithm, and the resulting phase values were quantized to 16 levels to facilitate the use of lithographic techniques for fabrication. Since the KPP phase profile is etched directly into fused silica, the finished product has a high laser-damage threshold at ultraviolet wavelengths (~18 J/cm$^2$ for 3-ns pulses at 351 nm). The experimentally measured far-field intensity pattern displays the desired top-hat envelope with superimposed speckle. The far field contains approximately 90% of the incident energy inside the designed 640-μm region. This is a significant improvement over the binary RPPs in terms of the far-field profile control and energy concentration.

## Iterative Algorithm for KPP Design

The ability to tailor the focal plane irradiance profile and increase its energy content is achieved at the expense of relaxing the binary phase and regular element assumptions of the RPPs. The fundamental issue in designing a continuous phase screen is to determine a phase pattern in the input plane that, for a given input intensity distribution, produces the desired far-field intensity distribution. In most cases, because the phase of the electric field in the far field is not of interest, it can be left arbitrary. This freedom in the far-field phase allows us to obtain a solution to the near-field phase screen problem. The problem of designing a continuous phase screen is similar to the phase-recovery problem[14] that has been investigated since the 1970s, and iterative algorithms have been developed to construct the required phase screens.

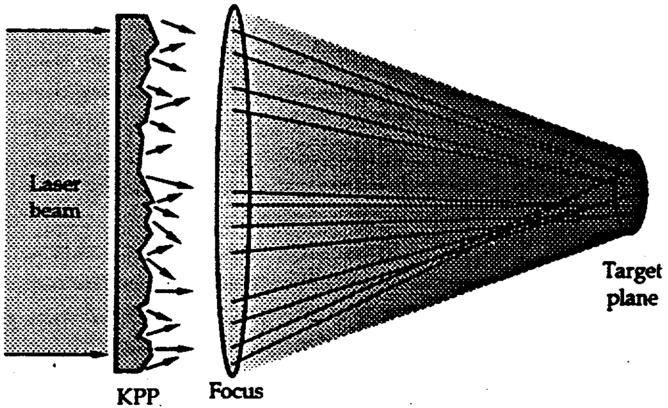

FIGURE 1. Geometric optic illustration of how a KPP tailors the focal plane irradiance profile. (70-50-0994-3431pb01)

The existence of a "phase-only" solution for this design problem can be understood as follows. The continuous phase screen can be approximated by small contiguous regions such that the phase varies linearly over each region. Each of these linearly varying phase regions acts like a small prism, or wedge, and steers that part of the incident beam to a spot in the far field, offset as determined by the wedge angle (Fig. 1). Thus, a desired focal plane intensity profile can be generated by a set of appropriately distributed wedge angles and sizes in the near field. We have developed an iterative algorithm that allows us to systematically design the required KPP phase screens.

In ICF applications, we envision placing these KPPs at the final focusing lens and expect to produce the desired irradiance profiles in the target plane at the lens focus. In a focusing geometry, the near-field amplitude $E_{\rm nf}(x', y')$ and the far field amplitude $E_{\rm ff}(x, y)$ (both complex) are related to each other through the Fourier transform[9,15]

$$E_{\rm ff}(\nu_x,\nu_y) = \frac{-i}{\lambda f}\int_{\text{input aperture}} dx'dy' \times \exp\left[\frac{-2\pi i}{\lambda f}(xx'+yy')\right]E_{\rm nf}(x'y') , \tag{1}$$

where $\nu_x = x/\lambda f$ and $\nu_y = y/\lambda f$ relate the far-field distances to the Fourier frequencies, $\lambda$ is the light wavelength, and $f$ is the lens focal length. The problem is to construct an input plane phase screen that, combined with a given input intensity distribution, produces a required far-field intensity distribution. As a specific example, we consider producing a supergaussian intensity profile in the far field from a supergaussian profile in the near field. Thus, the input-plane intensity profile is written as

$$I_{\rm nf}(x,y) = \exp\left[-\left(\frac{x^2+y^2}{r_0^2}\right)^n\right] , \tag{2}$$

where $r_0$ is the input beam radius. Similarly, the desired far-field profile is written as

$$I_{\rm ff}(x,y) = \exp\left[-\left(\frac{x^2+y^2}{r_{\rm f}^2}\right)^n\right] , \tag{3}$$

with $r_f$ being the far-field beam radius. For simplicity, we have assumed the powers of the near-field and far-field supergaussians to be equal. In general, the method works adequately for any reasonable integrable profiles within the limits of diffraction.

The phase screen design problem then can be stated as follows: Construct a near-field phase screen $\phi(x,y)$ [embedded in the complex amplitude $E_{nf}(x,y)$] that produces the far-field intensity profile in Eq. (3), given the near-field intensity profile in Eq. (2). To allow us to construct iteratively the phase screen $\phi(x,y)$, no constraints are placed on the phase in the far field.

Apparently, no general mathematical proof exists as to the existence or uniqueness of the solution to this problem. Clearly, the arbitrariness of the far-field phase would imply an infinite number of solutions (if one exists). However, iterative algorithms have been developed to solve a wide range of problems in image recovery and synthesis, speckle interferometry, beam-profile manipulation for microwave plasma heating, designing diffractive optical elements, etc.[16–18] We have numerically implemented such an iterative algorithm to construct phase screens for tailoring the far-field intensity distribution.

The general flow of the iterative algorithm is described in Fig. 2. We begin by choosing the near-field amplitude, given by the square root of Eq. (2) and a random phase screen. Taking the Fourier transform of this complex amplitude leads to an amplitude- and phase-modulated far-field distribution. At this point, the far-field constraint is applied to the amplitude, leaving the phase unchanged. Taking the inverse Fourier transform of this complex field gives the near-field distribution, which has both amplitude and phase modulations. Now, the near-field constraint is applied to the amplitude, leaving the phase unchanged. The procedure is repeated again by Fourier transforming to the far field, etc. This iteration loop continues until a desirable convergence is achieved or until a prescribed number of iterations (typically 50) is reached. As measures of convergence, we use (1) the root-mean-square deviation between the desired profile and that obtained by the iterative procedure and (2) the energy content in the far field.

The choice of the near-field and far-field constraints is dictated by the specific problem under investigation. Usually, the near-field intensity profile is known, and the natural near-field constraint is to replace the amplitude obtained during the iterative optimization with the square root of the near-field intensity [such as that given by Eq. (2)]. Examples of far-field constraints are (1) replacing the amplitude with the square root of the desired far-field intensity profile or (2) multiplying the far-field intensity with a weighting function of the form given in Eq. (3). We call these the *replacement* and *multiplicative* constraints, respectively. While the replacement constraint is the natural choice for generating a flat-top focal irradiance profile, we find that the multiplicative choice is particularly useful for ICF applications in which the primary interest is the energy content within a desired region in the far field and not the specific distribution of intensity within this region.

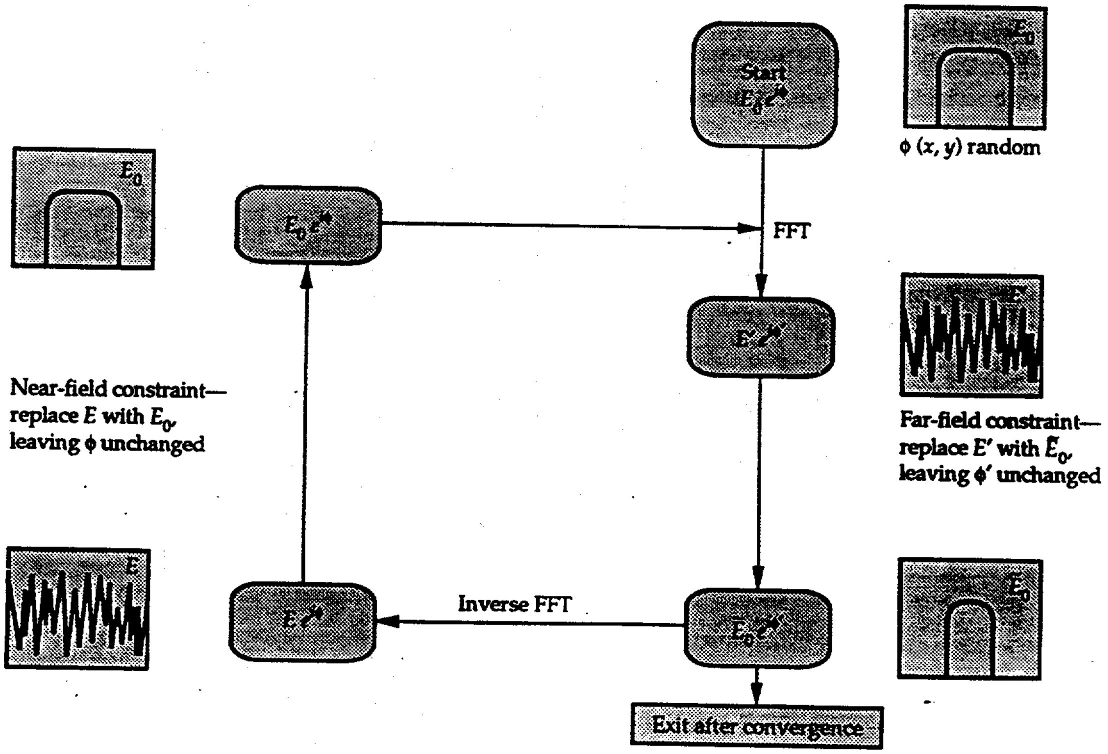

FIGURE 2. Iterative algorithm for designing the KPPs. (70-50-0994-3432pb01)

The converged focal profile with the multiplicative constraint usually is found to be very speckly in the region of interest. However, the far-field pattern obtained by using the multiplicative constraint is less sensitive to beam aberrations than that obtained by using the replacement constraint. A far-field irradiance generated using the replacement constraint changes to a speckle pattern with a very small amount of near-field aberrations. Although the multiplicative constraint is a more practical choice for ICF applications, for illustrative purposes in this article we have designed and fabricated KPP phase screens by using the replacement constraint in both the near field and the far field.

## Numerical Simulations

We have implemented the iterative algorithm to construct phase screens to tailor the far-field irradiance profiles. These simulations were carried out using fast Fourier transform (FFT) techniques on a 512 × 512 grid. For convenience in preparing the masks for KPP fabrication (see the next section), the pixel size in the near field was chosen to be 305 μm, and the radius of the near-field intensity profile, $r_0$, was chosen to be 5.5 cm. Then, the focal plane spatial resolution is 10.1 μm for $\lambda = 0.527$ μm, $f = 3$ m, and the far-field spatial extent is about 5.17 mm. The speckle size, which corresponds to the input beam diameter of 11 cm, is about 35 μm. The square pixels on the KPP lead to a large-scale, two-dimensional sinc$^2$ envelope pattern in the far-field. The desired top-hat profile is superimposed on this envelope pattern. For a 305-μm-square aperture of a single pixel in our case, the first zero of the sinc$^2$ envelope occurs at about 5 mm from the center. The far-field spot size, $r_f$, has to be considerably less than the far-field extent to minimize aliasing effects in the simulations and to reduce the energy loss in the secondary Airy maxima of a single-pixel diffraction pattern. In the numerical simulations that follow, we have chosen $r_f = 320$ μm and have verified theoretically that less than 1% of the incident energy is lost in the secondary maxima.

A typical KPP obtained after 50 iterations is shown in Fig. 3, and the expected far-field intensity profile produced by this KPP illuminated with an unaberrated beam is shown in Fig. 4. The overall shape of the far-field profile is quite close to the desired profile,

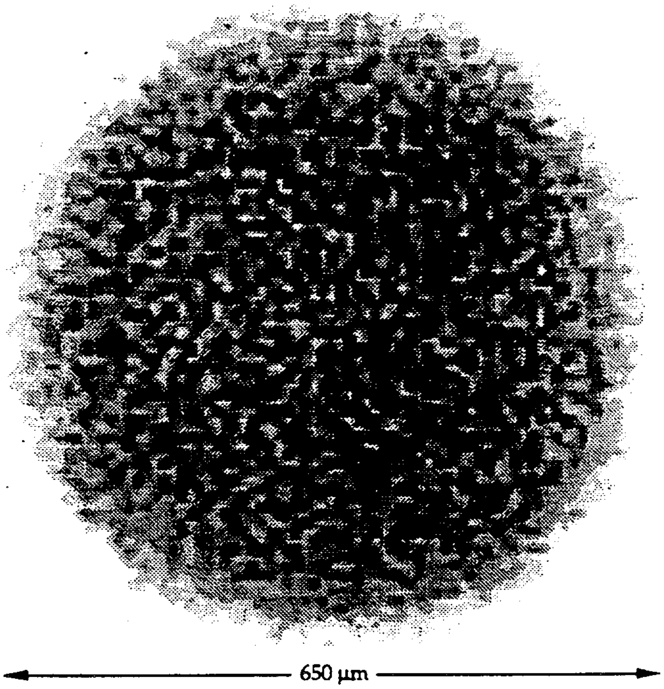

FIGURE 4. Far-field intensity profile produced by the KPP shown in Fig. 3(a). (70-50-0994-3435pb01)

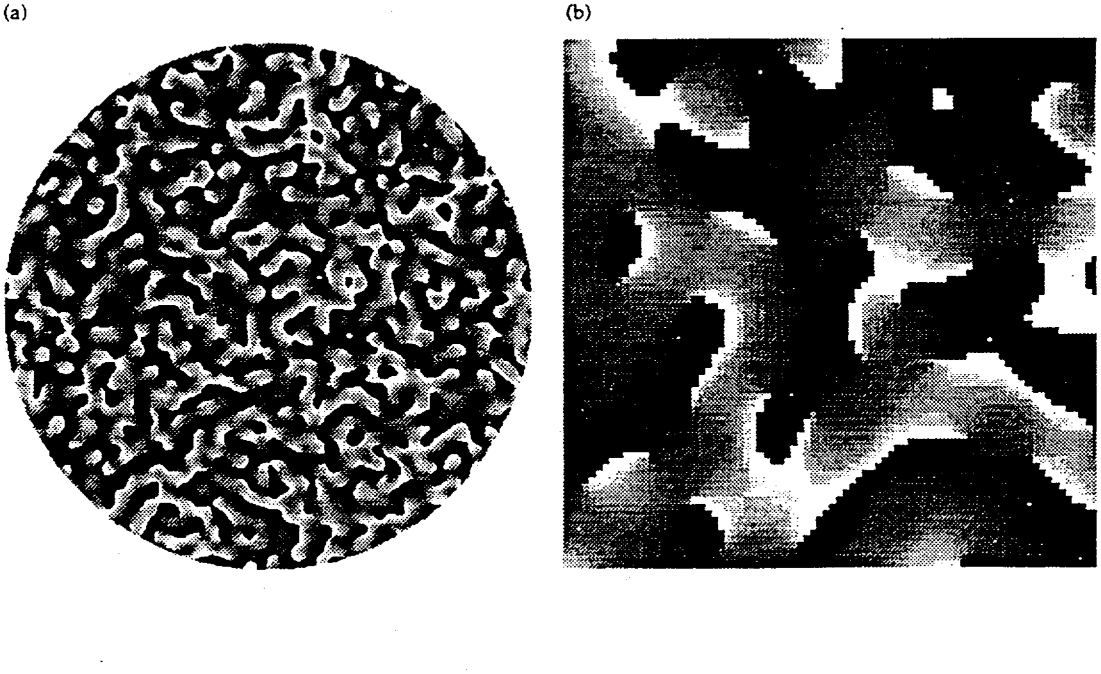

FIGURE 3. (a) Gray-scale representation of the KPP phase screen obtained after 50 iterations. The phase values range from 0 (black) to 2π (white). (b) Magnified section of the KPP phase screen. Gray scale is the same as in (a). The 2π phase jumps are characterized by the black-white discontinuities. (70-50-0994-3434pb01)

although some residual fluctuations remain. We find that most of the convergence occurs after the first few (five or so) iterations and slows considerably afterward. It is also interesting to note that, for a uniphase input beam, the modulations in the far-field profile are less than 100%. However, our calculations indicate that the beam aberrations increase the far-field intensity modulations, causing the intensity distribution to look more like a speckle pattern.

ICF applications demand, in addition to a desired far-field intensity profile, maximum energy containment within this profile. Figure 5 shows the fraction of the incident energy contained inside a circle of a given diameter as a function of that diameter. The improvement of the energy concentration with each iteration is clearly visible, as is the slow convergence after the first few cycles. The 640-μm-diam circle contains about 90% of the incident energy. This is a significant improvement over the regular-element, binary RPPs when the element size is chosen such that the size of the central maximum (to the first zero) is equal to the size of the supergaussian profile in the far field ($r_f$).

The near-field phase screen obtained after the iterative optimization [see Fig. 3(a)] shows a ripply structure resembling waves on a lake surface. A magnified display of a portion of the KPP phase screen [see Fig. 3(b)] indicates that the phase is fairly smooth except for discrete $2\pi$ jumps that result from determining the phase by means of the numerical arctangent function, which is limited to the range $-\pi$ to $\pi$. Some of the $2\pi$ jumps seem to occur as closed-loop lines, whereas others appear as open-loop lines (branch cuts). Endpoints of such open-loop $2\pi$ discontinuities correspond to locations where the complex electric field in the near field during the iteration sequence goes to zero. The phase values around such endpoint singularities rapidly climb from zero to $2\pi$. We have observed that these singularities lead to interesting intensity minima in the near-field diffraction following the KPP. This will be discussed in a later publication. Although it is straightforward to unwrap the closed-loop $2\pi$ jumps, it is not possible to unwrap the open-loop $2\pi$ branch cuts. We are currently investigating algorithms for constructing phase screens that do not contain such singularities.

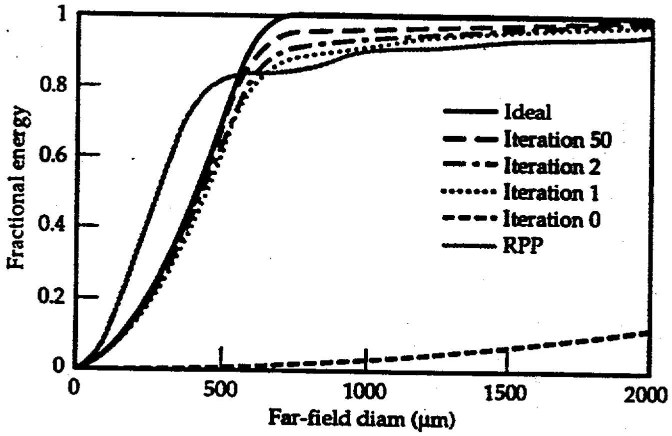

FIGURE 5. Evolution of the focal plane energy concentration with iteration. (70-50-0994-3436pb01)

## KPP Fabrication

The KPP was fabricated by means of lithographic techniques and wet-etching of fused silica in a buffered hydrofluoric acid solution. Here, $2^N$ phase levels can be fabricated by using $N$ binary-amplitude masks and varying the etch times with each mask. We quantized the computer-generated KPP phase screen containing phase values between 0 and $2\pi$ to 16 phase levels so that they could be fabricated using four binary-amplitude masks. Our calculations indicate that, for the present pixel size, a 16-level quantization results in about 1% more energy loss outside the desired region than does a continuous phase screen. Note that an unwrapped phase screen would be expected to be several waves deep and would thus require many more discrete levels to minimize phase-quantization errors. This would also add additional fabrication steps to the lithographic approach used here.

A $2\pi$ relative phase delay corresponds to an etch depth of $t = \lambda/(n-1)$, where $n$ is the refractive index at the operating wavelength $\lambda$. In the multiple-binary-mask approach, etching after exposure through mask 1 reaches depth $t/2$, that following mask 2 reaches depth $t/4$, the next one reaches $t/8$, and so on. A fabrication process consisting of $N$ masks yields $2^N$ phase levels (0 to $2^N - 1$), with a maximum etch depth $t = (1 - 1/2^N)$. Since the present KPP was fabricated for use at 527 nm, $t$ = 1146 nm ($n$ = 1.46 for fused silica), and the smallest etch depth was 72 nm.

In fabricating the 16-level KPP, we used a sequence of steps consisting of photoresist coating, exposing through the appropriate binary mask, developing the resist, and etching unprotected areas on the substrate to the required depth. Each sequence is similar to that used to fabricate binary RPPs in our laboratory, the main differences being that the sol-gel coating is absent and the etch time changes with each sequence. Approximately 120 nm of chrome was deposited on 1.5-cm-thick, 15-cm-diam, fused-silica substrates prior to the KPP fabrication. We cleaned the substrate with a UV/ozone treatment and used an adhesion promoter, hexamethyldisilizane, to ensure a good bond between the substrate and the photoresist and to avoid undercutting and peeling during the subsequent etching. A layer of photoresist (Shipley 1400) about 2 μm thick was spin-coated onto the substrate and fully exposed through the mask by using an extended white light source. The binary amplitude masks for each exposure stage were prepared using a Gerber photoplotter on acetate-based photographic film. The etching was done in a constant-temperature, buffered, hydrofluoric-acid solution (1% HF + 15% $NH_4F$) for up to 28 minutes. A similar procedure was reported recently for fabricating a 16-level, diffractive optical element for intensity-shaping a laser cavity mode.[19]

Accurate overlay of masks is crucial to obtaining sharp edges between the pixels on the KPP. Wider edges lead to large-angle scattering and hence to a reduction in the amount of energy contained within the central top-hat profile. We used three alignment fiducials written on the film at the edge of the KPP pattern to align the masks. The fiducials on masks 2, 3, and 4 were aligned, prior to exposure, with those initially patterned on the substrate from mask 1. We found that the masks made on acetate film lead to considerable overlay inaccuracy across the KPP aperture because of the flexibility of the film. We are now investigating how to minimize this error by producing the binary masks on rigid glass substrates. Figure 6(a) shows a white-light interferogram of the KPP, which exhibits various phase levels as gray scales. A magnified view of a small section of the KPP [Fig. 6(b)] shows the pixelated nature of the KPP phase screen. High-resolution microscope pictures of the edges indicate that some of the edges were very sharp (better than 2 µm), but others were very broad (about 20 µm). The wider edges resulted mainly from errors in the pixel size on the binary film masks and overlay inaccuracies, and less from the etch step. Based on relative area, we estimate a 1 to 2% loss in energy efficiency due to wide-angle scattering from these edges. The step heights of different phase levels were measured on four calibration strips fabricated at the edge of the KPP by means of a Dektak stylus profilometer. The average of the four step-height measurements is compared to the expected values in Fig. 7. The maximum relative deviation is about 10%, although most of the step heights are within 3% of the expected values. The absolute deviations in the measured step heights were on the order of ±10 nm.

## Optical Performance

We evaluated the optical performance of the KPP by measuring the far-field intensity profile and its energy content. The monochromatic output of an argon-ion laser at 514 nm was collimated, passed through the KPP, and focused through a lens with a 3-m focal length. The far-field image was recorded on film, digitized using a photodensitometer, and then processed

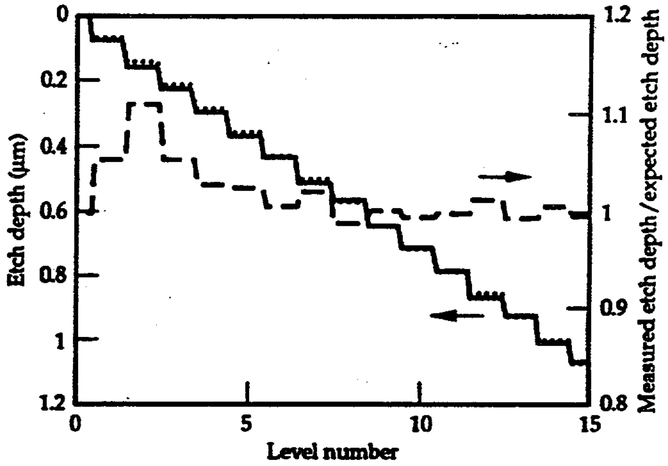

FIGURE 7. Comparison of measured step heights (solid line) to expected values (dotted line). Also shown is the ratio of the measured step heights to the expected step heights (dashed line). (70-50-0994-3438pb01)

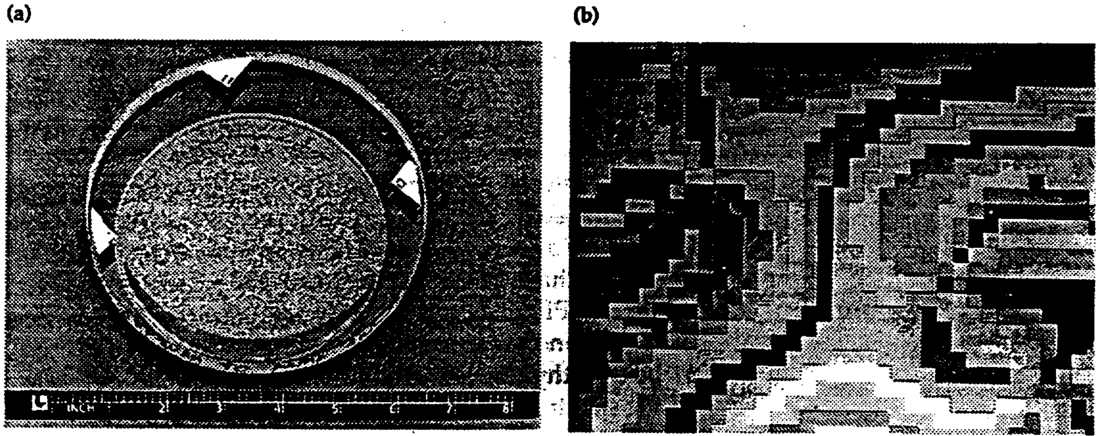

FIGURE 6. (a) White-light interferogram of the KPP. Various phase levels are displayed as different gray levels. (b) A magnified white-light interferogram image of a section of the KPP. Pixel size on the KPP is 305 µm. (70-50-0994-3437pb01)

to calculate the irradiance distribution. Figure 8(a) shows one such profile of focal plane intensity recorded on the film, and Fig. 8(b) shows a line-scan across the center of a processed image. Although the far-field image has a relatively coarse modulation for this small KPP, the ~640-µm-diam top-hat nature of the profile is evident. Figure 8(c) shows line scans through the far-field patterns calculated by using measured average step heights and illuminating the KPP with 514- and 527-nm coherent light. We see that illuminating the KPP with a coherent 514-nm laser is predicted to give a small (~4:1) coherent spike at the center of the far-field image because the KPP was designed for use at 527 nm. The rest of the far-field pattern and the energy content show insignificant differences between the two wavelengths. On the other hand, the experimental data in Fig. 8(b) do not show any significant coherent spike at the far-field center. We believe this is probably the result of imperfections in the actual step heights across the KPP and optical aberrations in the beam. The measured intensity pattern has an overlaid speckle with modulation depth comparable to that predicted. (The far-field speckle size for the fabricated KPP aperture is about 34 µm.) Details of the speckle in the two cases, however, would be expected to be different because even a small amount of aberrations would alter the speckle distribution in the far field.

In addition to the desired top-hat profile, we also observed a halo around the central pattern and the diffraction pattern of the individual 305-µm pixels extending to several orders in the horizontal and the vertical directions. These features are at much lower intensities than the desired central spot and thus are not visible in Fig. 8. The features caused by diffraction from a pixel can be eliminated by fabricating a continuously varying phase screen (as opposed to the pixelated one fabricated here). The halo also can be minimized in a discrete KPP by sharpening the pixel edges. (We are now fabricating KPPs with finer edge width.)

The energy concentration in the focal plane was determined by measuring the energy passing through pinholes of differing sizes, normalized to the total energy in a near-field plane following the KPP. This comparison removes the Fresnel reflection losses from the bare surfaces of the KPP. The measured energy concentration is compared with the calculated energy distribution in Fig. 9. The measured fractional energy values closely follow the theoretical values but seem to be about 5% below them. We believe that most of this deviation is caused by poor edge definition. Nevertheless, the 640-µm-diam region contains approximately 90% of the incident energy—a significant improvement over the binary RPP energy content of 82%.

## Summary and Further Improvements

In summary, we developed an iterative procedure to construct KPPs for producing desired far-field profiles with efficient energy concentration. The method is quite robust and is stable with regard to the type of the far-field profiles that can be generated. Numerical simulations indicate that the convergence is achieved after only a few iterations and that the resulting far-field profile contains more than 95% of the incident energy within the desired region.

We also fabricated a 16-level KPP on fused silica with a 12-cm-diam aperture using lithographic techniques and wet chemical etching. The measured far-field intensity pattern displays the expected top-hat envelope with a superimposed speckle and contains about 90% of the

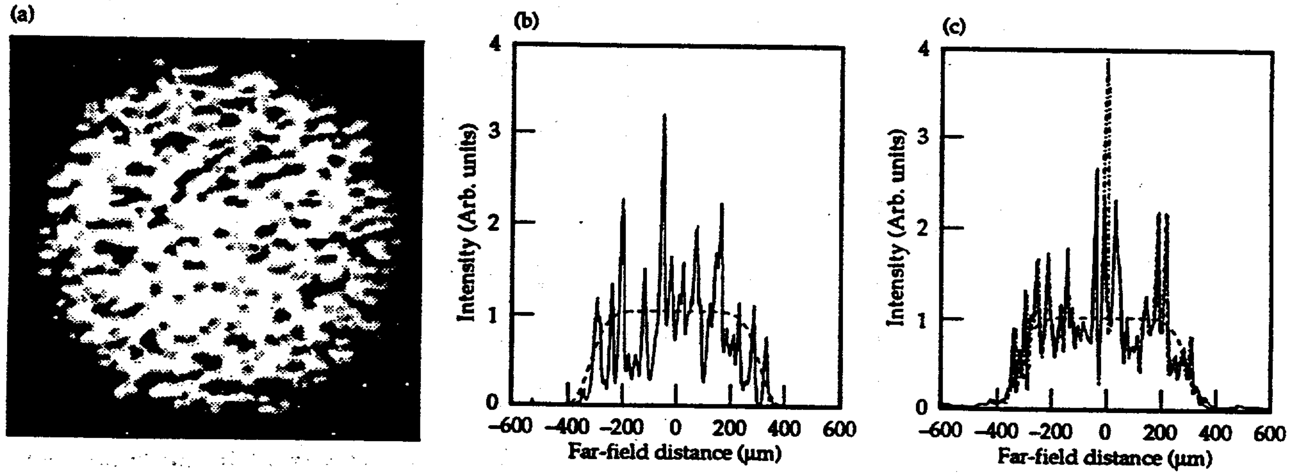

FIGURE 8. (a) Film image of the far-field intensity distribution produced by the KPP. (b) Horizontal line scan through the center of a far-field image such as the one shown in (a) following processing. The dashed line denotes the 8th-power supergaussian envelope. (c) Horizontal line scan through the center of the calculated KPP far-field pattern for illumination with 527-nm (solid line) and 514-nm (dot-dashed line) coherent light. Note the slight change in the far-field spatial scale for 514- and 527-nm wavelengths. The dashed line again denotes the 8th-power supergaussian envelope (shown for 527 nm). (70-50-0994-3441pb01)

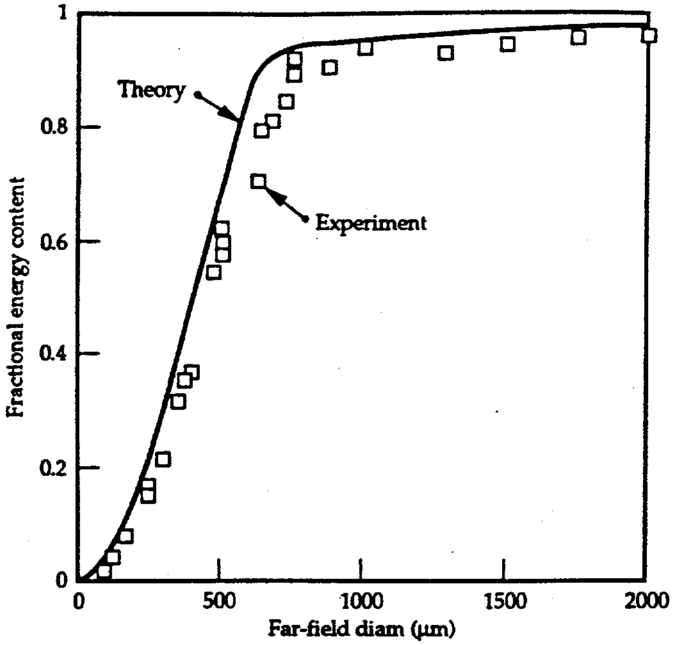

FIGURE 9. Energy concentration in the far field produced by the KPP. The solid line denotes the calculated energy concentration, and the data points correspond to the measured normalized energy passing through various-sized pinholes. (70-50-0994-3442pb01)

incident energy inside the designed 640-μm-diam region. This is a significant improvement over binary RPPs in terms of far-field profile control and energy concentration.

We anticipate several improvements in the design and fabrication of the KPPs. We believe that eliminating the open-loop, 2π jumps can improve KPP efficiency in the far field while minimizing near-field intensity modulations. Then, the phase screen could be unwrapped, and the method of fabrication could be chosen. Further increases in KPP efficiency will require the production of more accurate masks and better alignment and overlay controls. We are working on these aspects and are developing methods to scale up the technology for fabricating large-aperture (up to 65-cm-diam) KPPs for use on the Nova laser and on the proposed National Ignition Facility.

## Acknowledgments

We acknowledge collaborations with Janice Lawson and Ken Manes during the early phase of our KPP design and fabrication work. We also thank L. N. Manchester for assistance with generating the binary masks.

## Notes and References

1. J. D. Lindl, R. L. McCrory, and E. M. Campbell, "Progress toward ignition and burn propagation in inertial confinement fusion," *Phys. Today* 45, 32 (1992).
2. Y. Kato, K. Mima, N. Miyanaga, S. Arinaga, Y. Kitagawa, M. Nakatsuka, and C. Yamanaka, "Random phasing of high-power lasers for uniform target acceleration and plasma instability suppression," *Phys. Rev. Lett.* 53, 1057 (1984).
3. X. Deng, X. Liang, Z. Chen, W. Yu, and R. Ma, "Uniform illumination of large targets using a lens array," *Appl. Opt.* 25, 377 (1986).
4. R. M. Stevenson, M. J. Norman, T. H. Bett, D. A. Pepler, C. N. Danson, and I. N. Ross, "Binary zone plate arrays for the generation of uniform focal profiles," *Opt. Lett.* 19, 363 (1994).
5. S. Skupsky, R. W. Short, T. Kessler, R. S. Craxton, S. Letzring, and J. M. Soures, "Improved laser beam uniformity using the angular dispersion of frequency modulated light," *J. Appl. Phys.* 66, 3456 (1989).
6. R. H. Lehmberg and S. P. Obenschain, "Use of induced spatial incoherence for uniform illumination of laser fusion targets," *Opt. Commun.* 46, 27 (1983).
7. D. Veron, H. Ayral, C. Gouedard, D. Husson, J. Lauriou, O. Martin, B. Meyer, M. Rostaong, and C. Sauteret, "Optical spatial smoothing of Nd:Glass laser beam," *Opt. Commun.* 65, 42 (1988).
8. H. Nakano, K. Tsubakimoto, N. Miyanaga, M. Nakatsuka, T. Kanabe, H. Azechi, T. Jitsuno, and S. Nakai, "Spectrally dispersed amplified spontaneous emission for improving irradiation uniformity into high power Nd:glass laser system," *J. Appl. Phys.* 73, 2122 (1993).
9. H. T. Powell, S. N. Dixit, and M. A. Henesian, "Beam smoothing capability on the Nova laser," *ICF Quarterly Report* 1(1), 28, Lawrence Livermore National Laboratory, Livermore, CA, UCRL-LR-105821-91-1 (1990).
10. See, for example, M. Born and E. Wolf, *Principles of Optics* 6th edition (Pergamon, New York, 1980), p. 393.
11. S. N. Dixit, I. M. Thomas, B. W. Woods, A. J. Morgan, M. A. Henesian, P. J. Wegner, and H. T. Powell, "Random phase plates for beam smoothing on the Nova laser," *Appl. Opt.* 32, 2543 (1993).
12. S. N. Dixit, J. K. Lawson, K. R. Manes, H. T. Powell, and K. A. Nugent, "Kinoform phase plates for focal plane irradiance profile control," *Opt. Lett.* 19, 417 (1994).
13. S. N. Dixit, I. M. Thomas, M. Rushford, R. Merrill, M. D. Perry, and H. T. Powell, "Fused silica kinoform phase plates for generation of uniform focal plane irradiance profiles," submitted to *Opt. Lett.*
14. See, for example, R. W. Gerchberg and W. O. Saxton, "A practical algorithm for determination of phase from image and diffraction plane pictures," *Optik* 35, 237 (1972); J. R. Feinup, "Phase retrieval algorithms: a comparison," *Appl. Opt.* 21, 2758 (1982).
15. J. W. Goodman, *Introduction to Fourier Optics* (McGraw-Hill, New York, 1968), Ch. 5, p. 85.
16. N. C. Gallagher and B. Liu, "Method for computing kinoforms that reduces image reconstruction error," *Appl. Opt.* 12, 2328 (1973).
17. N. C. Gallagher and D. W. Sweeney, "Computer generated microwave kinoforms," *Opt. Eng.* 28, 599 (1989).
18. See for example, the papers in the Technical Digest for the conference Diffractive Optics: Design, Fabrication, and Applications, *1994 Technical Digest Series* 11 (Optical Society of America, Washington, DC, 1994).
19. J. R. Leger, D. Chen, and Z. Wang, "Diffractive optical element for mode shaping of a Nd:YAG laser," *Opt. Lett.* 19, 108 (1994).